

Deep Predictor-Corrector Networks for Robust Parameter Estimation in Non-autonomous System with Discontinuous Inputs

Gyeongwan Gu^{1*} Jinwoo Hyun^{2*} Hyeontae Jo^{1,2†} Jae Kyoung Kim^{2,3,4†}

Abstract

Learning under non-smooth objectives remains a fundamental challenge in machine learning, as abrupt changes in conditioning variables can induce highly non-smooth loss landscapes and destabilize optimization. This difficulty is particularly pronounced in non-autonomous dynamical systems driven by discontinuous inputs, where widely used optimization methods, including recent neural smoothing approaches, exhibit unreliable convergence or strong hyperparameter sensitivity. To address this issue, we propose Deep Predictor–Corrector Networks (DePCoN), a multi-scale learning framework that stabilizes optimization by learning scale-consistent parameter update rules across a hierarchy of smoothed inputs. Rather than treating smoothing as a fixed preprocessing choice, DePCoN integrates smoothing into the learning dynamics itself through a learned predictor–corrector mechanism. Across biological and ecological benchmarks with discontinuous inputs, DePCoN consistently achieves more robust and faster convergence than existing methods while substantially reducing sensitivity to hyperparameter choices. Beyond dynamical systems, our approach provides a general learning principle for stabilizing optimization under non-smooth objectives.

1. Introduction

Many machine learning models fail not only because of insufficient expressiveness, but also because of ill-posed

¹Department of Mathematics, Ajou University, Suwon 16499, Republic of Korea ²Biomedical Mathematics Group, Institute for Basic Science, Daejeon 34126, Republic of Korea ³Department of Mathematical Sciences, KAIST, Daejeon 34141, Republic of Korea ⁴Department of Medicine, College of Medicine, Korea University, Seoul 02841, Republic of Korea. Correspondence to: Hyeontae Jo <ajouhtj@ajou.ac.kr>, Jae Kyoung Kim <jaekkim@kaist.ac.kr>.

Preprint. March 16, 2026.

Table 1. Representative applications of non-autonomous dynamical systems driven by discontinuous exogenous inputs.

Category	Application	Input type (Reference)
Control	Traffic signals	Periodic redgreen switching (Aboudolas et al., 2009)
Bio/Life	NF- κ B signaling pathways	External stimuli (e.g. TNF- α) (Nelson et al., 2004)
Electronic engineering	Power electronics	Component faults (Domínguez-García & Trenn, 2010)
Finance	Financial control	Central bank interventions (Cadenillas & Zapatero, 2000)
Neural networks	Neural dynamics	Spiking synaptic activity (Stamov & Stamova, 2007)
Epidemiology	Non-pharmaceutical interventions	Discrete policy shocks (Flaxman et al., 2020)

optimization problem under non-smooth objectives (Goffin, 1977; Nesterov, 2005). In many practical settings, abrupt changes in inputs or conditioning variables can induce highly non-smooth loss landscapes, rendering widely used optimization methods unstable and unreliable. This challenge arises across a wide range of learning problems and persists even in low-dimensional settings.

A prominent instance of this challenge arises in non-autonomous differential equations, which are widely used to describe natural and engineered systems driven by time-varying exogenous inputs (Åström & Murray, 2021; Coppel, 1978). Such models support a broad range of tasks, including prediction, control, system design, optimization, and the evaluation of interventions or policy scenarios across scientific and engineering domains. In many real-world systems, these exogenous inputs are inherently non-smooth, as they are generated by switching rules, pulsed actions, or event-triggered decisions. This setting is encountered, for example, in control systems with red–green traffic-light switching or event-based demand response (Aboudolas et al., 2009; Du & Zhang, 2014; Mathieu et al., 2012; Chassin et al., 2015), in power electronics with high-frequency on–off switching (Papafotiou et al., 2004; Siddhartha et al., 2018), and in biological and circadian models involving bolus dosing, abrupt external stimulation, or light–dark forcing (Huang et al., 2012; Nelson et al., 2004; Forger et al., 1999; Song et al., 2023; Lim et al., 2025) (See Table 1 and Table 3 for representative examples).

Recent work has attempted to mitigate this issue by smoothing discontinuous inputs using kernels or neural network approximations and performing parameter estimation on the resulting surrogate dynamics (Beck & Teboulle, 2012; Yang & Fu, 2014; Lin et al., 2023; Ko et al., 2023; Xu, 2024). While such approaches can improve numerical stability in certain cases, they still rely on selecting a single smoothing scale or network configuration, making performance highly sensitive to the hyperparameter choice: insufficient smoothing fails to stabilize optimization, whereas excessive smoothing distorts the underlying dynamics and biases the recovered parameters. As a consequence, existing smoothing-based methods often trade optimization stability for estimation bias rather than resolving the core optimization difficulty.

In this paper, we introduce Deep Predictor–Corrector Networks (DePCoN), a multi-scale learning framework that stabilizes optimization under non-smooth objectives by learning scale-consistent update rules in parameter space. Rather than treating smoothing as a fixed preprocessing choice, DePCoN embeds smoothing into the learning dynamics itself by jointly leveraging a hierarchy of smoothed inputs. A learned predictor propagates parameter estimates across smoothing scales, while a corrector enforces data consistency at each scale through Neural ODE–based system identification. By aggregating estimation errors across scales, DePCoN transforms smoothing from a fragile hyperparameter into a structured learning input. We further provide a convergence analysis showing that, as the smoothing scale vanishes, the resulting sequence of optimal parameter estimates converges to the global minimizer under standard stability assumptions (Appendix B).

Through experiments on biological and ecological systems with discontinuous inputs, we show that DePCoN consistently achieves stable and accurate parameter estimation in regimes where widely used optimization and existing neural smoothing approaches fail. Beyond non-autonomous dynamical systems, our framework provides a general learning principle for stabilizing optimization under non-smooth objectives, with potential applications to a broad class of machine learning problems involving discontinuous conditioning or highly non-smooth loss landscapes.

2. Related Works

A common strategy to mitigate optimization difficulties induced by non-smooth objectives is to replace the original problem with a smooth surrogate that is easier to optimize (Beck & Teboulle, 2012). One approach is kernel-based smoothing, in which the input signal is regularized via convolution with a smoothing kernel. This construction follows a well-established principle in mathematical analysis, where convolution with an approximate identity yields

smooth approximations that converge to the original function as the smoothing scale decreases (see, e.g., (Friedrichs, 1944; Hwang & Jo, 2019) and Chapter 5 of (Evans, 2022)). Closely related ideas have also appeared in modern deep learning as continuation or homotopy-based optimization heuristics, where objective smoothing is used to reduce the ruggedness the loss landscape and stabilize training (Lin et al., 2023; Xu, 2025). In practice, however, the choice of the smoothing scale is critical: insufficient smoothing may fail to eliminate non-smoothness and lead to numerical instability, whereas excessive smoothing can distort the original dynamics and introduce systematic estimation bias.

More recently, neural-network-based smoothing approaches have been proposed, in which discontinuous exogenous inputs are approximated using neural networks with smooth activation functions, thereby inducing a smooth surrogate objective for parameter estimation. A representative example is Harmonic Approximation of Discontinuous External Signals using Neural Networks (HADES-NN) (Jo et al., 2026), which alternates between neural approximation of the input signal and parameter optimization on the resulting surrogate dynamics. While universal approximation results guarantee that such networks can approximate the target input in principle, the effective smoothness of the learned representation depends strongly on architectural and optimization hyperparameters, such as network depth, width, activation functions, and learning rates. As a consequence, neural-network-based smoothing such as HADES-NN can exhibit hyperparameter-dependent bias, producing surrogate dynamics that deviate from the original system even when the optimization procedure converges.

A common limitation shared by both kernel-based and neural-network-based smoothing approaches is that they rely on a single, implicitly chosen smoothing scale or effective smoothness level, making the resulting optimization sensitive to hyperparameter choices. Moreover, smoothing is typically treated as an auxiliary or preprocessing step, rather than being integrated into the learning dynamics of the parameter estimation process itself.

3. Main Results

3.1. Failure of Widely Used Optimizers under Discontinuous Forcing

We begin by revisiting a representative failure mode of parameter estimation in non-autonomous systems driven by discontinuous real-world inputs, as formulated in Equation (1), using the human circadian pacemaker model as an illustrative testbed (Figure 1-(a) i)). This model was already employed in previous work (Jo et al., 2026) to demonstrate that widely used optimization methods, including deep-learning-based approaches, can yield unstable and highly

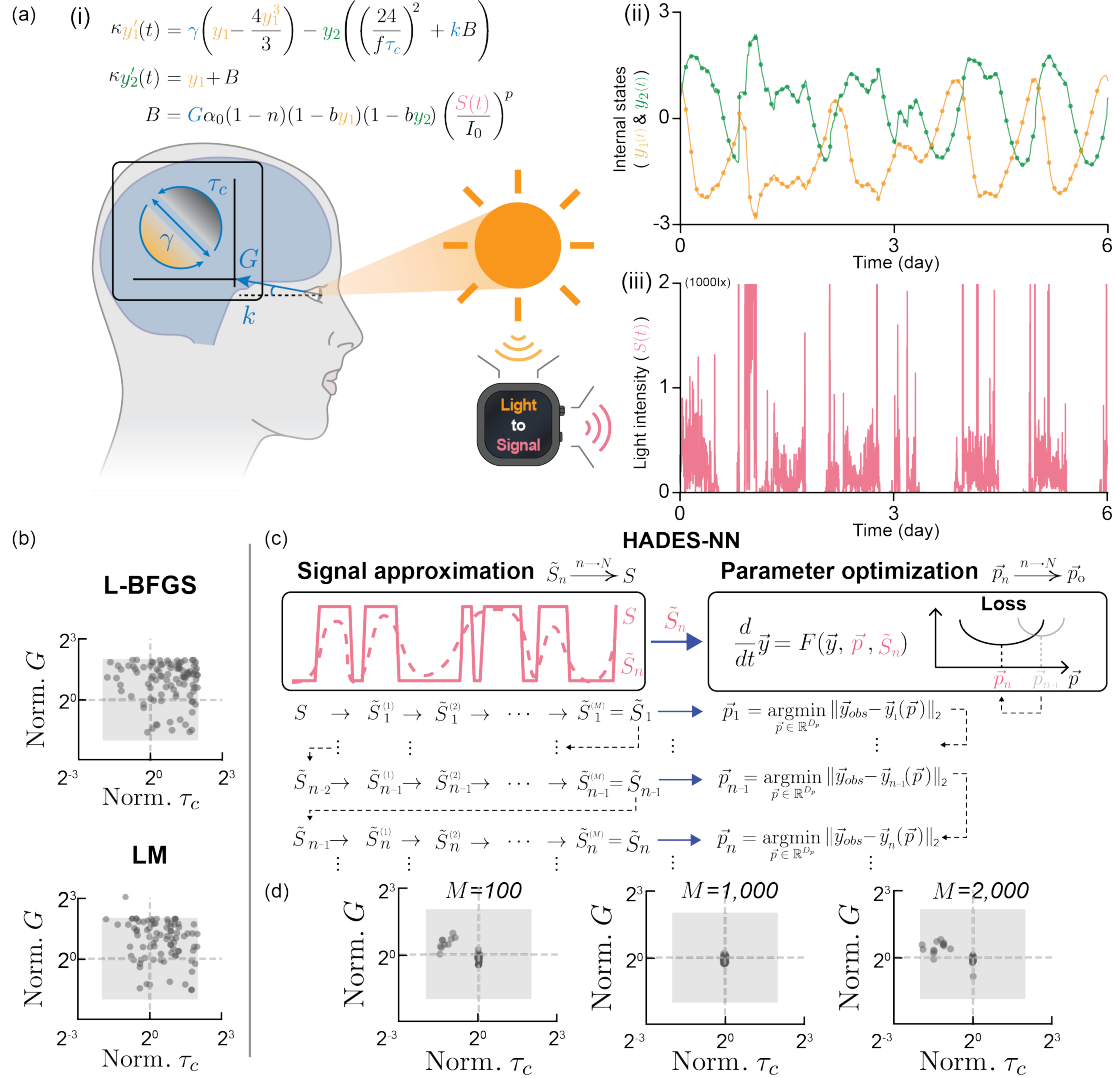


Figure 1. Failure of widely used local optimization under discontinuous inputs and hyperparameter sensitivity of HADES-NN. (a) Human circadian pacemaker model in which discontinuous light exposure $S(t)$ is transformed into an effective photic drive $B(t)$ and subsequently modulates the internal oscillator states $\vec{y}(t) = (y_1(t), y_2(t))$. (i) Synthetic observations are generated (ii) by integrating the system for 144 hours using real-world light measurements $S(t)$ (iii). (b) Scatter plots of parameter estimates obtained by widely used optimization methods, including L-BFGS and LM, from randomized initializations. The gray box indicates the range of parameters from which initial values were randomly sampled. All estimates are normalized by the true parameter values, which are located at the intersection of the dashed lines. Each point represents the final estimate from 30 independent optimization trials, illustrating large dispersion and unstable convergence under irregular exogenous inputs. (c) Schematic of HADES-NN, which alternates between neural smoothing of the discontinuous input and parameter optimization. At each outer iteration, a smoothed input \tilde{S}_n is refined through M inner updates and used to estimate system parameters. (d) Sensitivity of HADES-NN to the smoothing depth M . While increasing M enhances regularization, excessive smoothing suppresses informative input variations and induces estimation bias, whereas small M provides insufficient stabilization.

dispersed parameter estimates under irregular or abruptly switching exogenous signals.

The circadian pacemaker model is a mechanistic non-autonomous oscillator in which the wearable-derived light signal $S(t)$ is transformed into an effective photic drive $B(t)$ and subsequently coupled to the internal states $\vec{y}(t) = (y_1(t), y_2(t))$. Inter-individual variability in circadian responses is summarized by the set of four parameters $\vec{p} =$

$(p_1, p_2, p_3, p_4) = (\tau_c, \gamma, G, k)$, representing the intrinsic period, oscillator stiffness, photic gain, and coupling strength, respectively (see (Jo et al., 2026) for details). We numerically integrate the model over 144 hours (6 days) using the measured light exposure $S(t)$ as input and construct synthetic observation data by uniformly sampling 80 time points, $\{\vec{y}_o(t_i)\}_{i=1}^{80}$ (Figure 1-(a) ii-iii). Given these observations, we estimate \vec{p} that minimize a loss function Equa-

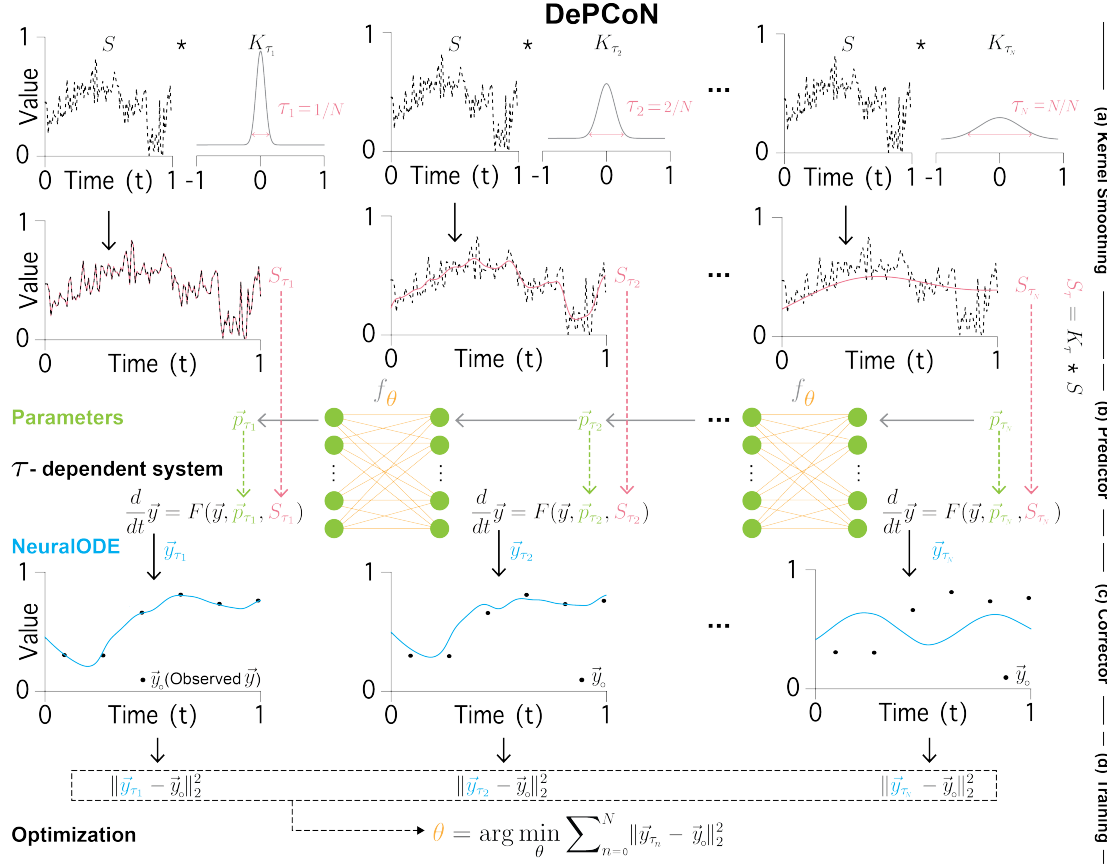


Figure 2. DePCoN stabilizes parameter estimation by learning parameter update rules that remain consistent across multiple input-smoothing scales. (a) Multi-scale preprocessing of the discontinuous exogenous input $S(t)$ via heat-kernel convolution, producing a hierarchy of smoothed inputs $\{S_{\tau_n}(t)\}_{n=0}^N$ with normalized scales $\tau_n = n/N$, from lightly smoothed (τ_1) to heavily smoothed (τ_N). (b) Predictor stage. Starting from the coarsest scale τ_N , the predictor network f_{θ} propagates parameter estimates toward finer scales according to $\vec{p}_{\tau_{n-1}} = f_{\theta}(\vec{p}_{\tau_n})$, transferring stable information to increasingly discontinuous regimes. (c) Corrector stage. For each scale τ_n , the predicted parameters \vec{p}_{τ_n} and smoothed input $S_{\tau_n}(t)$ define a τ -dependent non-autonomous system whose Neural ODE solution \vec{y}_{τ_n} is compared with observations. (d) Training objective. The predictor network is trained end-to-end by minimizing a multi-scale loss $\sum_{n=0}^N \|\vec{y}_{\tau_n} - \vec{y}_o\|$, enforcing consistency across scales and reducing sensitivity to any single smoothing choice.

tion (2). To assess robustness with respect to initialization, parameter estimation is repeated with random initial guesses sampled independently from $[p_{o,i}/4, 4p_{o,i}]$ for $i = 1, \dots, 4$ (gray boxes in Figure 1-(b)). Both Limited-memory Broyden–Fletcher–Goldfarb–Shanno (L-BFGS) and Levenberg–Marquardt (LM), despite being standard choices in practice, produce widely dispersed estimates across runs rather than consistently converging to the ground-truth parameters, indicated by the horizontal dashed line at the reference level $2^0 = 1$ (Figure 1-(b), Figure 5-(a)). This lack of convergence is not limited to gradient-based methods. As shown in Figure 5-(a), several widely used derivative-free or constrained optimization algorithms—including Differential Evolution (DE), Nelder–Mead (NM), and Sequential Least Squares Quadratic Programming (SLSQP)—also fail to recover meaningful parameter estimates under the same discontinuous-input setting. In particular, DE frequently diverges numerically, while NM and SLSQP remain trapped

near their initializations, yielding highly dispersed or systematically biased estimates.

These results are consistent with the failure mode reported in (Jo et al., 2026) and reflects a fundamental difficulty: discontinuous and irregular inputs induce highly non-smooth loss landscapes that degrade the performance of widely used optimization methods.

3.2. Hyperparameter Sensitivity of HADES-NN

Recently, HADES-NN was proposed to mitigate this issue by learning smooth approximations of discontinuous inputs $S(t)$ and performing parameter optimization using the resulting dynamics (Jo et al., 2026). HADES-NN alternates between signal smoothing and parameter optimization over an outer loop indexed by $n = 1, \dots, N$ (Figure 1-(c)). At the n -th outer iteration, a neural-network-based smoother refines a smoothed approximation of the discontinuous input

through M inner updates ($m = 1, \dots, M$), yielding a progressively refined signal $\tilde{S}_n^{(M)}$, denoted by \tilde{S}_n . Using this refined input \tilde{S}_n , HADES-NN integrates the corresponding dynamical system Equation (1) by replacing $S(t)$ with \tilde{S}_n and updates the parameter estimate by fitting simulated trajectories to the observations, yielding an optimized parameter vector \vec{p}_n . Crucially, successive outer iterations are coupled through a continuation mechanism: the refined input approximation \tilde{S}_n is used to initialize the next smoothing stage, while the estimated parameters \vec{p}_n serve as the initial condition for the subsequent parameter optimization.

To assess the sensitivity of HADES-NN to the smoothing depth, we evaluate parameter estimates obtained with different values of the inner-loop iteration number ($M = 100, 1000, \text{ and } 2000$, while fixing $N = 200$) (Figure 1-(d)). Although HADES-NN improves estimation accuracy over widely used optimization baselines (Figure 1-(b)), the results reveal a pronounced dependence on M . When M is small, insufficient regularization leads to increased dispersion of parameter estimates, whereas large M can over-smooth informative input variations and introduce bias.

In addition to accuracy sensitivity, increasing M incurs a non-negligible computational cost. Because each smoothing update requires repeated neural approximation and numerical integration, larger values of M substantially increase runtime. Together, these results indicate that the optimal choice of M is not obvious *a priori* and requires careful tuning to balance accuracy, robustness, and computational efficiency.

3.3. DePCoN: A Predictor–Corrector Framework for Parameter Estimation under Discontinuous Inputs

To overcome the hyperparameter sensitivity and computational burden observed in existing approaches, we propose *Deep Predictor–Corrector Networks (DePCoN)*, a parameter-estimation framework that integrates information across multiple smoothing scales in a principled manner. Rather than relying on a single smoothed input, DePCoN exploits a hierarchy of smoothed signals and learns scale-consistent parameter updates, leading to stable estimation under discontinuous exogenous inputs.

As illustrated in Figure 2, DePCoN consists of a preprocessing step followed by two coupled stages: a predictor stage and a corrector stage. In the preprocessing step (Figure 2-(a)), we apply heat-kernel convolution to the discontinuous input signal $S(t)$ to generate a family of smoothed signals $\{S_{\tau_n}(t)\}_{n=0}^N$ Equation (3). The smoothing scale is normalized and discretized as $\tau_n = n/N$ for $n = 0, 1, \dots, N$, producing a hierarchy of inputs ranging from unsmoothed ($\tau_0 = 0$), through lightly smoothed ($\tau_1 = 1/N$), to heavily smoothed ($\tau_N = 1$) (See Section 4.2 for the mathematical interpretation of the case $\tau_0 = 0$).

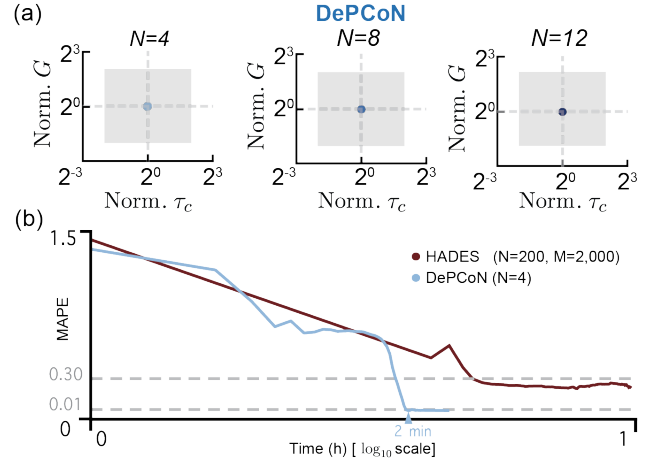


Figure 3. Hyperparameter robustness and computational efficiency of DePCoN. (a) Parameter estimation results of DePCoN under different smoothing-grid sizes $N = \{4, 8, 12\}$. Each panel shows the distribution of estimated parameters (τ_c, G) obtained from randomized initializations. In contrast to the pronounced hyperparameter sensitivity observed for HADES-NN in Fig. 1(d), the estimates produced by DePCoN remain tightly concentrated across all values of N , indicating substantially reduced sensitivity to the smoothing-grid hyperparameter. Gray boxes indicate the parameter ranges used for random initialization, and all estimates are normalized by the true parameter values, located at the intersection of the dashed lines. (b) MAPE trajectories over a 1-hour interval comparing DePCoN with HADES-NN. DePCoN rapidly enters a low-error regime and exhibits stable convergence, whereas HADES-NN converges more slowly and remains at a higher error level.

The predictor stage (Figure 2-(b)) learns to propagate parameter estimates across smoothing scales. Starting from the coarsest scale τ_N , the predictor network f_θ sequentially generates parameter estimates along the scale hierarchy according to $\vec{p}_{\tau_{n-1}} = f_\theta(\vec{p}_{\tau_n})$ for $n = 1, \dots, N$ (see architectural details in Section 4.3). Through this process, the predictor transfers stable parameter information obtained under heavy smoothing to finer scales where the effects of discontinuities are more pronounced.

In the corrector stage (Figure 2-(c)), the predicted parameters $\{\vec{p}_{\tau_n}\}_{n=0}^N$ are evaluated against the observations across all smoothing scales. For each scale τ_n , the smoothed input $S_{\tau_n}(t)$ together with the corresponding parameter estimate \vec{p}_{τ_n} defines a τ -dependent non-autonomous dynamical system Equation (4), whose Neural ODE solution is denoted by \vec{y}_{τ_n} . The discrepancy between \vec{y}_{τ_n} and the observed data \vec{y}_o provides a scale-specific estimation error (See Section 4.4 for the detailed formulation).

Crucially, the predictor network f_θ is trained end-to-end by minimizing the aggregated estimation error across all scales, i.e., by minimizing $\sum_{n=0}^N \|\vec{y}_{\tau_n} - \vec{y}_o\|$ Equation (5)–Equation (6). This multi-scale loss enforces consistency

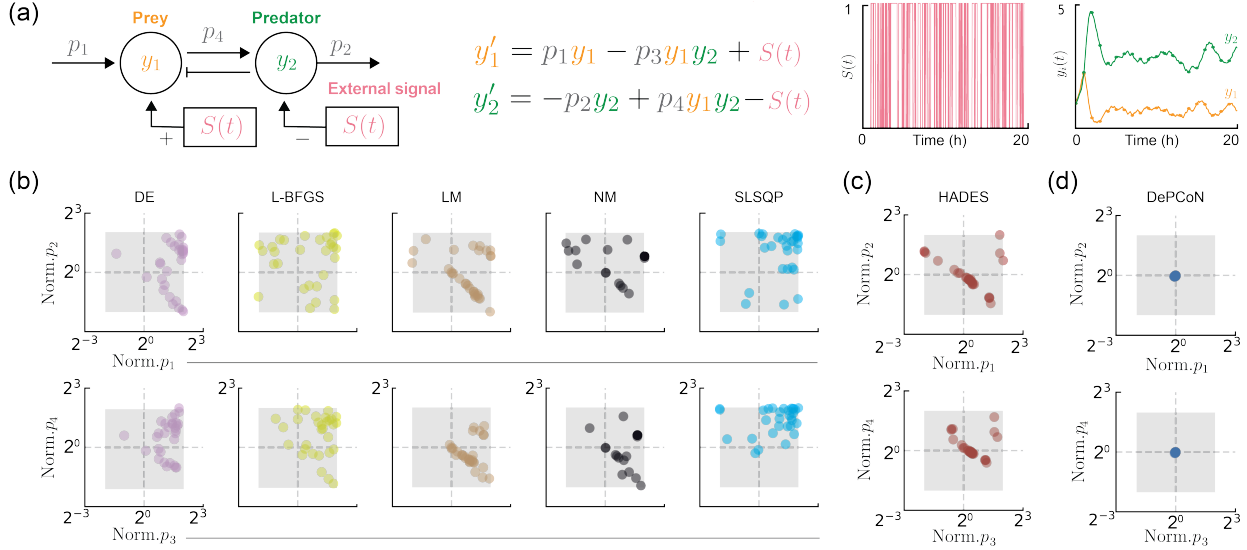


Figure 4. Robust parameter estimation on the Lotka–Volterra system with discontinuous exogenous inputs. (a) Modified Lotka–Volterra model describing prey–predator dynamics driven by an abrupt external signal $S(t)$. The resulting trajectories exhibit pronounced non-smooth behavior under real-world–like environmental perturbations. (b) Parameter estimates obtained using widely used optimization methods under identical experimental settings. Each scatter plot shows estimates of parameter pairs from 30 independent trials with randomized initializations, revealing broad dispersion and strong sensitivity to initialization. (c) Results for HADES–NN using hyperparameter configurations reported to perform well in prior studies (Jo et al., 2026). Despite neural smoothing of the discontinuous input, the resulting estimates remain unstable and exhibit systematic bias away from the ground-truth parameters. (d) DePCoN yields tightly clustered parameter estimates centered at the ground truth, demonstrating both high accuracy and strong consistency. All parameter estimates are normalized by the true parameter values, which are located at the intersection of the dashed lines, and gray boxes indicate the parameter ranges used for random initialization.

of parameter estimates across smoothing scales and couples the predictor and corrector stages in a unified learning framework. We also include mathematical analysis, under well-posed system assumption, the limit of \vec{p}_τ converges to the optimal parameter in Appendix B

3.4. Hyperparameter Robustness of DePCoN

As shown in Figure 1-(d), HADES–NN exhibits pronounced sensitivity to the smoothing hyperparameter. Motivated by this limitation, we investigate how the performance of the proposed DePCoN framework depends on its smoothing hyperparameter choices. To this end, we examine the parameter estimation behavior of DePCoN across different values of the smoothing-grid size $N = 4, 8, \text{ and } 12$ (Figure 3-(a)). Unlike HADES–NN, whose estimation accuracy varies significantly with the inner-loop iteration number M , the estimates produced by DePCoN remain consistently concentrated as N varies, indicating substantially reduced hyperparameter sensitivity. See also Figure 6-(a), which summarizes DePCoN’s sensitivity to the choice of N using box plots of the mean absolute percentage error (MAPE; Section A.3) over the range $N = 4, \dots, 12$.

We next evaluate the computational efficiency of HADES–NN and DePCoN under different number of inner-loop iteration (HADES–NN) and smoothing scales (DePCoN). To this end, we plot MAPE profiles over a 1-hour time interval

on the circadian pacemaker model (Figure 3-(b)), showing that DePCoN rapidly enters a low-error regime, reaching a MAPE of approximately 0.01 within the first 0.03h, and maintains stable convergence thereafter. In contrast, HADES–NN converges more slowly and saturates at substantially higher error levels (MAPE=0.3), requiring longer optimization to reach comparable accuracy. Together, these results demonstrate that DePCoN not only reduces sensitivity in the final parameter estimates but also accelerates convergence while stabilizing the overall optimization trajectory under hyperparameter variation.

Table 2 summarizes the parameter estimation results for the circadian pacemaker model. For each method, we report the mean \pm standard deviation of the estimated parameter values across independent trials, together with the overall MAPE. Consistent with the dispersion patterns observed in Figures 1 and 5, DePCoN yields estimates that are both accurate and stable, whereas the other methods exhibit large variability or systematic deviation from the ground truth.

3.5. Robust and Consistent Parameter Estimation on a Lotka–Volterra Benchmark

We next evaluate DePCoN on a non-autonomous Lotka–Volterra (LV) system, describing the interaction between prey (y_1) and predator (y_2) under a time-varying environment driven by $S(t)$, such as climate change, environmental

pollution, and human intervention (Figure 4-(a)). Such environment changes can vary abruptly, and also yields non-smooth trajectories $\vec{y} = (y_1, y_2)$ (Figure 4-(a) right). This LV system serves as a benchmark example in which discontinuous external inputs are known to severely degrade the performance of gradient-based parameter estimation. Although the LV model itself is relatively simple, it has been widely used to demonstrate the instability of optimization under discontinuous forcing, including in the benchmark study of (Jo et al., 2026). This makes it a suitable testbed for assessing robustness rather than expressive power.

While the original benchmark considered $S(t)$ applied only to y_1 , introducing opposing effects on both states further exacerbates non-smoothness in the loss landscape. Under this modified setting, We apply a range of widely used optimization methods (DE, L-BFGS, LM, NM, SLSQP, and HADES-NN). Notably, HADES-NN is evaluated using hyperparameters reported to perform well in prior studies. Even under this favorable condition, none of the methods reliably recover the ground-truth parameters Figure 4-(b-d). We then compare DePCoN with these six algorithms under identical experimental conditions. Each method is evaluated over 30 independent trials with parameters initialized uniformly from $[p_{o,i}/4, 4p_{o,i}]$ for $i = 1, \dots, 4$.

The results show that DePCoN is the only method that consistently yields estimates tightly clustered around the ground-truth parameters, as indicated by the concentration near the dashed-line intersection (Figure 4-(d)). This behavior reflects both high accuracy and strong consistency across random initializations. In contrast, competing methods exhibit either broad dispersion or systematic bias away from the ground truth, highlighting their sensitivity to both initial conditions and discontinuous inputs (Figure 4-(b-c)). In addition to the scatter plots in Figure 4-(d), Table 2 (Lotka Volterra) reports per-parameter estimation results (mean \pm standard deviation) and overall MAPE, showing that DePCoN consistently outperforms all baselines.

We further examine the sensitivity of DePCoN to the choice of the smoothing-grid size N using box plots of MAPE (See Figure 6 (b) for details). Across a wide range of values ($N = 4, \dots, 12$), the MAPE distributions remain remarkably stable, with no significant performance degradation as N varies. Although increasing N yields a denser set of smoothing scales and slightly higher computational cost, estimation accuracy remains largely invariant. These results demonstrate that DePCoN achieves stable and reliable parameter estimation on a benchmark system where discontinuous inputs render conventional and smoothing-based methods highly sensitive to hyperparameter choices.

4. Methodology

4.1. Description of the general non-autonomous differential equations with time-varying exogenous input $S(t)$

A system under the exogenous input, $S : [0, T] \rightarrow \mathbb{R}$, can generally be described by a non-autonomous differential equation with $F : \mathbb{R}^{d_y} \times \mathbb{R}^{d_p} \times \mathbb{R} \rightarrow \mathbb{R}^{d_y}$:

$$\frac{d}{dt}\vec{y} = F(\vec{y}, \vec{p}, S) \quad (1)$$

where $\vec{y}(t; \vec{p}) = \vec{y}(t) \in \mathbb{R}^{d_y}$ denote system state of our interest at time t , $\vec{p} \in \mathbb{R}^{d_p}$ is unknown parameter vector that determine the shape of \vec{y} . Fitting the solution of system Equation (1) to real observations requires the optimal choice of \vec{p} so that the resulting trajectory matches the observation data $\{\vec{y}_o(t_i) : i = 1, \dots, N_o\}$ on a finite time points $0 = t_1 < \dots < t_{N_o} = T$. This task is commonly formulated as a parameter estimation (inverse) problem: find an optimal \vec{p} that minimizes the following loss function measuring the discrepancy between the solution \vec{y} of Equation (1) and \vec{y}_o at observation times $\{t_i\}_{i=1}^{N_o}$:

$$\begin{aligned} L(\vec{p}) &= \frac{1}{N_o} \sum_{i=1}^{N_o} \|\vec{y}(t_i; \vec{p}) - \vec{y}_o(t_i)\|_2^2, \\ &= \frac{1}{N_o} \sum_{i=1}^{N_o} \sum_{j=1}^{d_y} |y_j(t_i; \vec{p}) - y_{o,j}(t_i)|^2. \end{aligned} \quad (2)$$

Under this setting, we denote \vec{p}_o by the minimizer of Equation (2). As noted in the introduction, this optimization problem is challenging in practice because the discontinuities in S can make the map $\vec{p} \mapsto L(\vec{p})$ highly irregular.

4.2. Generation of a family of smoothed input via Heat-kernel convolution

We propose the Heat-kernel-based smoothing method. Specifically, let $K_\tau(t) = \frac{1}{\sqrt{4\pi\tau}} \exp\left(-\frac{t^2}{4\tau}\right)$ denote the heat kernel with a diffusion time $\tau > 0$, (i.e., a smoothing scale: larger τ yields stronger smoothing) (Evans, 2022). To define the convolution on \mathbb{R} , we extend the input $S : [0, T] \rightarrow \mathbb{R}$ by zero outside $[0, T]$. We then define S_τ as the convolution of S with K_τ :

$$S_\tau(t) = (K_\tau * S)(t) = \int_{-\infty}^{\infty} K_\tau(t-s) S(s) ds, \quad \forall \tau > 0. \quad (3)$$

By construction, the heat-kernel convolution yields a smooth input $S_\tau \in C^\infty(\mathbb{R})$. Moreover, as $\tau \rightarrow 0^+$, $S_\tau \rightarrow S$ in the appropriate function-space sense (see Appendix B and (Stein & Shakarchi, 2009)). Finally, by selecting $N + 1$ discrete values of τ on $[0, 1]$, $\{\tau_n = n/N\}_{n=0}^N$, we obtain a family of smoothed inputs $\{S_{\tau_n}\}_{n=0}^N$ with $S_{\tau_0} = S$ (Figure 2-(a)).

Table 2. Quantitative comparison of parameter estimation results. Mean \pm standard deviation of estimated parameter values and overall MAPE across independent trials for DePCoN, HADES-NN (Jo et al., 2026), and widely used optimization methods (DE (Price et al., 2006), L-BFGS (Zhu et al., 1997), LM (Moré, 2006), NM (Gao & Han, 2012), SLSQP (Kraft, 1988)).

Systems	Param.	True	DePCoN (ours)	HADES-NN	DE	L-BFGS	LM	NM	SLSQP
Circadian pacemaker	τ_c	24	23.65\pm0.14	23.10 \pm 2.53	– \pm –	51.08 \pm 27.43	51.08 \pm 27.43	51.08 \pm 27.43	52.18 \pm 31.42
	G	20	19.85\pm0.30	19.59 \pm 1.21	– \pm –	46.34 \pm 20.58	46.34 \pm 20.58	46.34 \pm 20.58	49.34 \pm 24.07
	γ	0.23	0.23\pm0.00	0.28 \pm 0.08	– \pm –	0.52 \pm 0.26	0.52 \pm 0.26	0.52 \pm 0.26	0.50 \pm 0.30
	k	0.55	0.53\pm0.01	0.72 \pm 0.31	– \pm –	1.09 \pm 0.64	1.09 \pm 0.64	1.09 \pm 0.64	1.06 \pm 0.82
	MAPE		0.02\pm0.01	0.16 \pm 0.24	– \pm –	1.34 \pm 0.48	1.34 \pm 0.48	1.34 \pm 0.48	1.46 \pm 0.43
Lotka Volterra	p_1	2	1.97\pm0.03	3.00 \pm 1.92	5.97 \pm 2.00	4.02 \pm 2.70	4.17 \pm 2.16	5.51 \pm 3.06	5.04 \pm 2.50
	p_2	0.5	0.49\pm0.01	0.56 \pm 0.38	0.83 \pm 0.52	1.01 \pm 0.61	0.60 \pm 0.42	0.85 \pm 0.33	1.27 \pm 0.61
	p_3	1	0.99\pm0.01	1.47 \pm 0.68	2.45 \pm 0.74	2.27 \pm 1.02	2.03 \pm 0.74	2.55 \pm 0.83	2.25 \pm 1.14
	p_4	1	0.99\pm0.01	1.19 \pm 0.57	1.71 \pm 0.95	1.93 \pm 1.05	0.91 \pm 0.49	1.26 \pm 0.58	2.81 \pm 1.07
	MAPE		0.02\pm0.01	0.53 \pm 0.56	1.37 \pm 0.62	1.29 \pm 0.58	0.84 \pm 0.51	1.22 \pm 0.53	1.65 \pm 0.62

4.3. Development of the predictor network

We introduce a predictor network f_θ with trainable parameters θ (Figure 2-(b)), implemented as a fully connected neural network. Given the parameter estimate \vec{p}_{τ_n} , the predictor produces the next estimate at the smoothing scale τ_{n-1} , $\vec{p}_{\tau_{n-1}} = f_\theta(\vec{p}_{\tau_n})$, $\forall n = 1, \dots, N$. To this end, at the coarsest scale τ_N , we initialize the parameter \vec{p}_{τ_N} by sampling it from the admissible set P_o (see Assumption B.1 for details). Starting from the coarsest level τ_N , we feed \vec{p}_{τ_N} into f_θ . The first layer maps \vec{p}_{τ_N} to a 64 nodes via a linear transformation followed by a ReLU activation. This operation is then repeated through two additional hidden layers with 32 and 16 units, respectively, each followed by a ReLU activation, yielding a final 16-dimensional feature vector. The output layer is a single fully connected linear layer (no activation) that maps the final 16 features to the next parameter estimate $\vec{p}_{\tau_{N-1}}$ at smoothing scale τ_{N-1} . Repeating this procedure recursively generates $\{\vec{p}_{\tau_n}\}_{n=0}^{N-1}$ (Figure 2-(b) Parameters).

4.4. Development of the corrector network

Although the predictor yields a sequence of parameter estimates $\{\vec{p}_{\tau_n}\}_{n=0}^N$, these predictions are not, in general, optimal for any well-defined objective at each smoothing level yet. We therefore introduce a correction step. For each smoothing scale τ_n , given the predicted parameter \vec{p}_{τ_n} from the previous step, we first compute the state trajectory \vec{y}_{τ_n} by solving the τ -dependent non-autonomous system (Figure 2-(b)):

$$\frac{d}{dt}\vec{y} = F(\vec{y}, \vec{p}, S_{\tau_n}). \quad (4)$$

In practice, the solution operator for Equation (4) is implemented using a Neural ODE solver (Chen et al., 2018), which enables end-to-end differentiable evaluation of \vec{y}_{τ_n} and supports gradient-based updates of both \vec{p}_{τ_n} and the predictor parameters θ via adjoint-based backpropagation

(Figure 2-(c), NeuralODE).

We then quantify, for each smoothing scale τ , the discrepancy between \vec{y}_τ and \vec{y}_o by evaluating the following τ -dependent loss at observation times:

$$L_\tau(\vec{p}) = \frac{1}{N_o} \sum_{i=1}^{N_o} \|\vec{y}_\tau(t_i; \vec{p}) - \vec{y}_o(t_i)\|_2^2, \quad (5)$$

for $\tau = \tau_0, \dots, \tau_N$ (Figure 2-(c) Optimization). We then aggregate the losses across smoothing levels to obtain the multi-scale objective

$$\sum_{n=0}^N L_{\tau_n}(\vec{p}) = \frac{1}{N_o} \sum_{n=0}^N \sum_{i=1}^{N_o} \|\vec{y}_{\tau_n}(t_i; \vec{p}) - \vec{y}_o(t_i)\|_2^2. \quad (6)$$

Finally, we update both the predictor parameters θ and the terminal parameter \vec{p}_{τ_N} using the Adam optimizer. We repeat this predictor-corrector procedure until the gradient $\nabla_\theta \sum_{n=0}^N L_{\tau_n}(\vec{p}_{\tau_n})$ becomes sufficiently small.

5. Conclusion

Our results demonstrate that DePCoN consistently achieves stable and accurate parameter estimation under discontinuous inputs, outperforming widely used optimization methods, together with neural smoothing approaches in terms of robustness and time-to-accuracy. Beyond the specific setting of non-autonomous dynamical systems, DePCoN offers a general learning principle for stabilizing optimization under non-smooth objectives. By integrating heat-kernel convolution into the learning dynamics and enforcing consistency across scales, our framework transforms a traditionally fragile hyperparameter choice into a structured learning input. This perspective is broadly applicable to machine learning problems involving discontinuous conditioning, hybrid dynamics, or highly non-smooth loss landscapes.

References

- Aboudolas, K., Papageorgiou, M., and Kosmatopoulos, E. Store-and-forward based methods for the signal control problem in large-scale congested urban road networks. *Transportation Research Part C: Emerging Technologies*, 17(2):163–174, 2009.
- Åström, K. J. and Murray, R. *Feedback systems: an introduction for scientists and engineers*. Princeton university press, 2021.
- Bainov, D. and Dishliev, A. Population dynamics control in regard to minimizing the time necessary for the regeneration of a biomass taken away from the population. *ESAIM: Mathematical Modelling and Numerical Analysis*, 24(6): 681–691, 1990.
- Beck, A. and Teboulle, M. Smoothing and first order methods: A unified framework. *SIAM Journal on Optimization*, 22(2):557–580, 2012.
- Bielecki, T. R. and Pliska, S. R. Risk sensitive asset management with transaction costs. *Finance and Stochastics*, 4(1):1–33, 2000.
- Brezis, H. and Brézis, H. *Functional analysis, Sobolev spaces and partial differential equations*, volume 2. Springer, 2011.
- Brogliato, B. *Nonsmooth impact mechanics: models, dynamics and control*. Springer, 1996.
- Cadenillas, A. and Zapatero, F. Classical and impulse stochastic control of the exchange rate using interest rates and reserves. *Mathematical Finance*, 10(2):141–156, 2000.
- Carter, T. Optimal impulsive space trajectories based on linear equations. *Journal of optimization theory and applications*, 70(2):277–297, 1991.
- Carter, T. E. Necessary and sufficient conditions for optimal impulsive rendezvous with linear equations of motion. *Dynamics and control*, 10(3):219–227, 2000.
- Chassin, D. P., Stoustrup, J., Agathoklis, P., and Djilali, N. A new thermostat for real-time price demand response: Cost, comfort and energy impacts of discrete-time control without deadband. *Applied Energy*, 155:816–825, 2015.
- Chen, R. T., Rubanova, Y., Bettencourt, J., and Duvenaud, D. K. Neural ordinary differential equations. *Advances in neural information processing systems*, 31, 2018.
- Clarida, R., Gali, J., and Gertler, M. Monetary policy rules and macroeconomic stability: evidence and some theory. *The Quarterly journal of economics*, 115(1):147–180, 2000.
- Coppel, W. A. *Dichotomies in Stability Theory*, volume 629 of *Lecture Notes in Mathematics*. Springer, Berlin, Heidelberg, 1 edition, 1978. ISBN 978-3-540-08536-2. doi: 10.1007/BFb0067780.
- Domínguez-García, A. D. and Trenn, S. Detection of impulsive effects in switched daes with applications to power electronics reliability analysis. In *49th IEEE Conference on Decision and Control (CDC)*, pp. 5662–5667. IEEE, 2010.
- Du, L. and Zhang, Y. Positive switched system approach to traffic signal control for oversaturated intersection. *Discrete Dynamics in Nature and Society*, 2014(1):381567, 2014.
- Evans, L. C. *Partial differential equations*, volume 19. American mathematical society, 2022.
- Flaxman, S., Mishra, S., Gandy, A., Unwin, H. J. T., Mellan, T. A., Coupland, H., Whittaker, C., Zhu, H., Berrah, T., Eaton, J. W., et al. Estimating the effects of non-pharmaceutical interventions on covid-19 in europe. *Nature*, 584(7820):257–261, 2020.
- Forger, D. B., Jewett, M. E., and Kronauer, R. E. A simpler model of the human circadian pacemaker. *Journal of biological rhythms*, 14(6):533–538, 1999.
- Friedrichs, K. O. The identity of weak and strong extensions of differential operators. *Transactions of the American Mathematical Society*, 55(1):132–151, 1944.
- Gao, C., Li, K., Feng, E., and Xiu, Z. Nonlinear impulsive system of fed-batch culture in fermentative production and its properties. *Chaos, Solitons & Fractals*, 28(1): 271–277, 2006.
- Gao, F. and Han, L. Implementing the nelder-mead simplex algorithm with adaptive parameters. *Computational Optimization and Applications*, 51(1):259–277, 2012.
- Goffin, J. L. On convergence rates of subgradient optimization methods. *Mathematical Programming*, 13(1): 329–347, 1977. doi: 10.1007/BF01584346.
- Heydari, M. B., Zolfaghari, M., Asgari, M., and Jafari, N. Analysis of two modified goubau waveguides at thz frequencies: Conical and elliptical structures. *Optik*, 189: 148–158, 2019.
- Huang, M., Li, J., Song, X., and Guo, H. Modeling impulsive injections of insulin: towards artificial pancreas. *SIAM Journal on Applied Mathematics*, 72(5):1524–1548, 2012.
- Hwang, H. J. and Jo, H. The diffusive limit of the vlasov-fokker-planck equation with the chemotactic sensitivity

- coupled to a parabolic equation. *Journal of Mathematical Analysis and Applications*, 477(2):1224–1242, 2019.
- Ibrahim, R. A. *Vibro-impact dynamics: modeling, mapping and applications*, volume 43. Springer Science & Business Media, 2009.
- Jo, H., Josić, K., and Kim, J. K. Neural network-based parameter estimation for nonautonomous differential equations with discontinuous signals. *SIAM Journal on Applied Mathematics*, 86(1):327–347, 2026. doi: 10.1137/25M1741340. URL <https://doi.org/10.1137/25M1741340>.
- Khalil, H. K. and Grizzle, J. W. *Nonlinear systems*, volume 3. Prentice hall Upper Saddle River, NJ, 2002.
- Ko, J.-H., Koh, H., Park, N., and Jhe, W. Homotopy-based training of neuralodes for accurate dynamics discovery. *Advances in Neural Information Processing Systems*, 36: 64725–64752, 2023.
- Kraft, D. A software package for sequential quadratic programming. *Forschungsbericht- Deutsche Forschungs- und Versuchsanstalt für Luft- und Raumfahrt*, 1988.
- Lim, D., Choi, S. J., Song, Y. M., Park, H. R., Joo, E. Y., and Kim, J. K. Enhanced circadian phase tracking: A 5-h dlmo sampling protocol using wearable data. *Journal of Biological Rhythms*, 40(3):249–261, 2025.
- Lin, X., Yang, Z., Zhang, X., and Zhang, Q. Continuation path learning for homotopy optimization. In *International Conference on Machine Learning*, pp. 21288–21311. PMLR, 2023.
- Liu, C. and Sun, C. Robust parameter identification of a nonlinear impulsive time-delay system in microbial fed-batch process. *Applied Mathematical Modelling*, 111: 160–175, 2022.
- Mathieu, J., Dyson, M., Callaway, D., and Rosenfeld, A. Using residential electric loads for fast demand response: The potential resource and revenues, the costs, and policy recommendations. In *ACEEE Summer Study on Energy Efficiency in Buildings*, pp. 189–203. Citeseer, 2012.
- Meng, X., Li, Z., and Nieto, J. J. Dynamic analysis of michaelis–menten chemostat-type competition models with time delay and pulse in a polluted environment. *Journal of mathematical chemistry*, 47(1):123–144, 2010.
- Moline, D., Wagner, J., and Volk, E. Model of a mechanical clock escapement. *American Journal of Physics*, 80(7): 599–606, 2012.
- Moré, J. J. The levenberg-marquardt algorithm: implementation and theory. In *Numerical analysis: proceedings of the biennial Conference held at Dundee, June 28–July 1, 1977*, pp. 105–116. Springer, 2006.
- Nelson, D., Ihekweaba, A., Elliott, M., Johnson, J., Gibney, C., Foreman, B., Nelson, G., Sée, V., Horton, C., Spiller, D., et al. Oscillations in $\text{nf-}\kappa\text{b}$ signaling control the dynamics of gene expression. *Science*, 306(5696):704–708, 2004.
- Nesterov, Y. Smooth minimization of non-smooth functions. *Mathematical Programming*, 103(1):127–152, 2005. doi: 10.1007/s10107-004-0552-5.
- Nie, L., Peng, J., Teng, Z., and Hu, L. Existence and stability of periodic solution of a lotka–volterra predator–prey model with state dependent impulsive effects. *Journal of Computational and Applied Mathematics*, 224(2):544–555, 2009a.
- Nie, L., Teng, Z., Hu, L., and Peng, J. The dynamics of a lotka–volterra predator–prey model with state dependent impulsive harvest for predator. *Biosystems*, 98(2):67–72, 2009b.
- Papafotiou, G., Geyer, T., and Morari, M. Hybrid modelling and optimal control of switch-mode dc-dc converters. In *2004 IEEE Workshop on Computers in Power Electronics, 2004. Proceedings.*, pp. 148–155. IEEE, 2004.
- Price, K., Storn, R. M., and Lampinen, J. A. *Differential evolution: a practical approach to global optimization*. Springer Science & Business Media, 2006.
- Shen, B., Zhai, J., Gao, J., Feng, E., and Xiu, Z. Nonlinear state-dependent impulsive system and its parameter identification in microbial fed-batch culture. *Applied Mathematical Modelling*, 40(2):1126–1136, 2016.
- Siddhartha, V., Hote, Y. V., and Saxena, S. Non-ideal modelling and imc based pid controller design of pwm dc-dc buck converter. *IFAC-PapersOnLine*, 51(4):639–644, 2018.
- Song, X., Huang, M., and Li, J. Modeling impulsive insulin delivery in insulin pump with time delays. *SIAM Journal on Applied Mathematics*, 74(6):1763–1785, 2014.
- Song, Y. M., Choi, S. J., Park, S. H., Lee, S. J., Joo, E. Y., and Kim, J. K. A real-time, personalized sleep intervention using mathematical modeling and wearable devices. *Sleep*, 46(9):zsad179, 2023.
- Stamov, G. T. and Stamova, I. M. Almost periodic solutions for impulsive neural networks with delay. *Applied Mathematical Modelling*, 31(7):1263–1270, 2007.
- Stamov, G. T., Alzabut, J. O., Atanasov, P., and Stamov, A. G. Almost periodic solutions for an impulsive delay

model of price fluctuations in commodity markets. *Non-linear Analysis: Real World Applications*, 12(6):3170–3176, 2011.

Stamova, I. and Emmenegger, J.-F. Stability of the solutions of impulsive functional differential equations modelling price fluctuations in single commodity markets. *International Journal of Applied Mathematics*, 15:271–290, 2004.

Stein, E. M. and Shakarchi, R. *Real analysis: measure theory, integration, and Hilbert spaces*. Princeton University Press, 2009.

Tang, S. and Xiao, Y. One-compartment model with michaelis-menten elimination kinetics and therapeutic window: an analytical approach. *Journal of Pharmacokinetics and Pharmacodynamics*, 34(6):807–827, 2007.

Westervelt, E. R., Grizzle, J. W., and Koditschek, D. E. Hybrid zero dynamics of planar biped walkers. *IEEE transactions on automatic control*, 48(1):42–56, 2003.

Xu, C. Global optimization with a power-transformed objective and gaussian smoothing. *arXiv preprint arXiv:2412.05204*, 2024.

Xu, C. Global optimization with a power-transformed objective and gaussian smoothing. In *Forty-second International Conference on Machine Learning, 2025*. URL <https://openreview.net/forum?id=6ojzpdczIY>.

Yang, F. and Fu, C.-L. A mollification regularization method for the inverse spatial-dependent heat source problem. *Journal of computational and applied mathematics*, 255:555–567, 2014.

Ye, H., Gao, J., and Ding, Y. A generalized gronwall inequality and its application to a fractional differential equation. *Journal of Mathematical Analysis and Applications*, 328(2):1075–1081, 2007.

Zhu, C., Byrd, R. H., Lu, P., and Nocedal, J. Algorithm 778: L-bfgs-b: Fortran subroutines for large-scale bound-constrained optimization. *ACM Transactions on mathematical software (TOMS)*, 23(4):550–560, 1997.

Impact Statement

This paper presents work whose goal is to advance the field of Machine Learning for scientific applications. There are many potential societal consequences of our work, none of which we feel must be specifically highlighted here.

Acknowledgements

We do not include acknowledgements in the initial version of the paper submitted for blind review.

A. Preliminaries

A.1. Notation

Let $\vec{p} = (p_1, p_2, \dots, p_{d_p}) \in \mathbb{R}^{d_p}$ denote a real-valued vector of dimension $d_p \geq 1$. We measure its magnitude using the L^2 (Euclidean) norm:

$$\|\vec{p}\|_2 = \left(\sum_{i=1}^{d_p} p_i^2 \right)^{1/2}.$$

For a time-dependent vector $\vec{y}(t) = (y_1(t), y_2(t), \dots, y_{d_y}(t)) \in \mathbb{R}^{d_y}$ defined on $t \in [0, T]$, we use the pointwise L^2 norm

$$\|\vec{y}(t)\|_2 = \left(\sum_{i=1}^{d_y} y_i^2(t) \right)^{1/2}.$$

A.2. Function spaces

$\mathcal{L}^2(X)$ denotes the set of real-valued Lebesgue measurable functions defined on $X \subset \mathbb{R}^{d_x}$ $f : X \rightarrow \mathbb{R}$ such that $\|f\|_{\mathcal{L}^2(X)} := \left(\int_X |f(t)|^2 dt \right)^{1/2} < \infty$.

For vector-valued functions $\vec{y} : X \rightarrow \mathbb{R}^{d_y}$, same notations are used: $\|\vec{y}\|_{\mathcal{L}^2(X)} := \left(\sum_{i=1}^{d_y} \int_X y_i^2(t) dt \right)^{1/2} < \infty$.

A.3. Mean absolute percentage error

We evaluate parameter-estimation accuracy using the mean absolute percentage error (MAPE) and its averaged variants. Let $\vec{p}_o = (p_{o,1}, \dots, p_{o,d_p}) \in \mathbb{R}^{d_p}$ denote the ground-truth parameter vector and $\vec{p}_j = (p_{j,1}, \dots, p_{j,d_p})$ the estimate obtained from the j -th independent trial ($j = 1, \dots, K$). We define the elementwise absolute percentage error (APE) as

$$\text{APE}_{j,i} = \frac{|p_{j,i} - p_{o,i}|}{|p_{o,i}|}, \quad i = 1, \dots, d_p.$$

The MAPE is then defined by averaging over parameters and trials:

$$\text{MAPE} = \frac{1}{K} \sum_{j=1}^K \frac{1}{d_p} \sum_{i=1}^{d_p} \text{APE}_{j,i}.$$

B. Convergence of DePCoN estimates $\vec{p}_\tau \rightarrow \vec{p}_o$ as $\tau \rightarrow 0^+$

paragraphPurpose of the analysis. The following convergence analysis shows that, under standard well-posedness and identifiability assumptions, the sequence of optimal parameter estimates obtained at each smoothing scale is well-defined and converges to the optimizer of the unsmoothed problem as the smoothing vanishes. While this result assumes access to the scale-wise optima and therefore does not model the exact training dynamics of DePCoN, it provides the theoretical rationale for smoothing-based continuation: in practice, DePCoN learns to track these scale-wise optima across multiple smoothing levels and, at the finest scale, produces the final estimate by inferring the $\tau = 0$ parameter through the learned predictor network.

Let $(\vec{y}_o(t), \vec{p}_o, S(t))$ denote the observation trajectory, the ground-truth (optimal) parameter associated with Equation (2), and the given exogenous input, respectively. The underlying true system is

$$\frac{d}{dt} \vec{y}_o(t) = F(\vec{y}_o(t), \vec{p}_o, S(t)). \quad (7)$$

Although observations are available only at finitely many time points, we treat them as a continuous-time trajectory for notational simplicity and theoretical clarity; the same argument applies to the discretized setting.

For each $\tau > 0$, let $\vec{y}_\tau(t) = \vec{y}_\tau(t; \vec{p})$ denote the solution of the τ -dependent system Equation (4),

$$\frac{d}{dt}\vec{y}_\tau(t) = F(\vec{y}_\tau(t), \vec{p}, S_\tau(t)),$$

and let $\vec{y}(t) = \vec{y}(t; \vec{p})$ denote the solution of Equation (1). By Equation (7), we have $\vec{y}(t; \vec{p}_o) = \vec{y}_o(t)$.

In practice, the parameter estimates \vec{p}_τ are obtained by training DePCoN in the correction stage by minimizing Equation (5). In this section, we show that \vec{p}_τ converges to the ground-truth parameter \vec{p}_o in the vanishing-smoothing limit $\tau \rightarrow 0^+$. This convergence analysis also motivates the prediction stage of DePCoN, which propagates parameter estimates across smoothing scales. To establish the result, we impose the following assumptions, which ensure stability of the dynamical system.

Assumption B.1. [Admissible set and nondegenerate stationary branch] For each $\tau > 0$, let \vec{p}_τ denote a selected local minimizer of the (continuous-time) τ -dependent loss L_τ in Equation (5):

$$L_\tau(\vec{p}) = \|\vec{y}_\tau(\cdot; \vec{p}) - \vec{y}_o(\cdot)\|_{\mathcal{L}^2([0, T])}^2. \quad (8)$$

We assume that there exists a nonempty compact set $P_o \subset \mathbb{R}^{d_p}$ such that

$$\{\vec{p}_\tau\}_{\tau > 0} \subset P_o.$$

Moreover, there exists $\tau_* > 0$ such that the selected branch $\{\vec{p}_\tau\}_{0 < \tau \leq \tau_*}$ consists of nondegenerate stationary points. That is, for all $0 < \tau \leq \tau_*$,

$$\nabla_{\vec{p}} L_\tau(\vec{p}_\tau) = \vec{0}, \quad \nabla_{\vec{p}}^2 L_\tau(\vec{p}_\tau) \text{ is invertible.}$$

We adopt Assumption B.1 because the parameters \vec{p}_τ typically represent domain-specific quantities (e.g., physical or biological constants) whose plausible ranges are often known a priori. In our examples, we set

$$P_o = \left[\frac{1}{4}p_{o,1}, 4p_{o,1} \right] \times \cdots \times \left[\frac{1}{4}p_{o,d_p}, 4p_{o,d_p} \right].$$

Accordingly, such bounds can be imposed directly in the optimization procedure, preventing \vec{p}_τ from leaving the admissible set P_o and excluding nonphysical regimes.

The nondegeneracy condition on the stationary branch $\{\vec{p}_\tau\}$ is imposed to ensure local identifiability and stability of the minimizers with respect to perturbations in τ . In particular, invertibility of the Hessian $\nabla_{\vec{p}}^2 L_\tau(\vec{p}_\tau)$ rules out flat directions and guarantees that the stationary points are isolated.

Assumption B.2. [Well-posedness and regularity of F in Equation (1)] There exist constants $C_1, C_2 > 0$ such that, for all $\vec{p} \in P_o$, $\vec{y}, \vec{y}_1, \vec{y}_2 \in \mathbb{R}^{d_y}$, and $S, S_1, S_2 \in \mathbb{R}$,

$$\begin{aligned} \|F(\vec{y}_1, \vec{p}, S) - F(\vec{y}_2, \vec{p}, S)\|_2 &\leq C_1 \|\vec{y}_1 - \vec{y}_2\|_2, \\ \|F(\vec{y}, \vec{p}, S_1) - F(\vec{y}, \vec{p}, S_2)\|_2 &\leq C_2 |S_1 - S_2|. \end{aligned}$$

Under Assumption B.2, for each $\vec{p} \in P_o$ and each initial condition, the initial value problem Equation (1) admits a unique solution $\vec{y}(\cdot; \vec{p})$ on $[0, T]$. Consequently, the loss $L(\vec{p})$ is well-defined.

In addition, F is continuously differentiable with respect to (\vec{y}, \vec{p}) on $\mathbb{R}^{d_y} \times P_o \times \mathbb{R}$, and its partial derivatives $\partial_{\vec{y}} F$ and $\partial_{\vec{p}} F$ are locally bounded on this set.

Assumption B.3. [Optional: identifiability and local stability of the parameter] Given the input $S \in \mathcal{L}^2([0, T])$ and the observation trajectory $\vec{y}_o(t)$, consider the continuous-time loss $L(\vec{p})$ in Equation (2):

$$L(\vec{p}) = \|\vec{y}(\cdot; \vec{p}) - \vec{y}_o(\cdot)\|_{\mathcal{L}^2([0, T])}^2, \quad (9)$$

where $\vec{y}(\cdot; \vec{p})$ denotes the solution of Equation (1) under parameter \vec{p} . In general, the minimizer of Equation (9) need not be unique, so $\arg \min_{\vec{p} \in P_o} L(\vec{p})$ is naturally viewed as a set of minimizers. We assume that L admits a unique global minimizer $\vec{p}_o \in P_o$, i.e., $\arg \min_{\vec{p} \in P_o} L(\vec{p}) = \vec{p}_o$, and that L satisfies a quadratic growth condition at \vec{p}_o : there exist a constants $c > 0$ such that

$$L^{1/2}(\vec{p}) \geq L^{1/2}(\vec{p}_o) + c \|\vec{p} - \vec{p}_o\|_2^2, \quad \forall \vec{p} \in P_o.$$

Assumption B.3 is optional but conceptually decisive. It encodes identifiability and well-conditioning: the uniqueness of \vec{p}_o rules out structural non-identifiability (multiple parameters producing indistinguishable trajectories), while the quadratic growth condition excludes flat directions near the optimum. As a result, convergence statements for \vec{p}_τ bifurcate depending on whether Assumption B.3 is imposed. Without Assumption B.3, one can typically guarantee only that $\{\vec{p}_\tau\}_{\tau>0}$ has accumulation points in P_o and that every limit point belongs to the set of global minimizers $\arg \min_{\vec{p} \in P_o} L(\vec{p})$; in contrast, under Assumption B.3, the limit is forced to be the single identifiable parameter \vec{p}_o .

Under Assumptions B.1–B.3, we show that, as $\tau \rightarrow 0^+$, the minimizers $\{\vec{p}_\tau\}_{\tau>0} \subset P_o$ of the τ -dependent loss L_τ in Equation (5) converge to the ground-truth parameter \vec{p}_o . The proof is organized into four steps:

Step B.1 (Input mollification) As $\tau \rightarrow 0^+$, $\|S_\tau - S\|_{\mathcal{L}^2(\mathbb{R})} \rightarrow 0$, by Lemma B.4 and Corollary B.5. Obviously, this implies $\|S_\tau - S\|_{\mathcal{L}^2([0,T])} \rightarrow 0$.

Step B.2 (Stability of trajectories) Fix $\vec{p} \in P_o$, and let $\vec{y}_\tau(\cdot; \vec{p})$ and $\vec{y}(\cdot; \vec{p})$ be the solutions of Equation (4) and Equation (1), respectively. Under Assumption B.2,

$$\|S_\tau - S\|_{\mathcal{L}^2([0,T])} \rightarrow 0 \quad \text{implies} \quad \|\vec{y}_\tau(\cdot; \vec{p}) - \vec{y}(\cdot; \vec{p})\|_{\mathcal{L}^2([0,T])} \rightarrow 0,$$

by Step B.1 and Lemma B.6.

Step B.3 (Stability of the loss) If $\tau \rightarrow 0^+$, then

$$\|L_\tau^{1/2} - L^{1/2}\|_{\mathcal{L}^2(P_o)} \rightarrow 0,$$

by Step B.2 and Corollary B.7, where $L_\tau(\vec{p})$ and $L(\vec{p})$ are defined in Equation (8) and Equation (9), respectively.

Step B.4 (Convergence of minimizers). (i) *Without Assumption B.3.* The stability of the objectives implies convergence in optimal value:

$$\lim_{\tau \rightarrow 0^+} L(\vec{p}_\tau) = L(\vec{p}_o),$$

and hence every accumulation point of $\{\vec{p}_\tau\}_{\tau>0}$ (which exists up to subsequence by compactness of P_o in Assumption B.1) is a global minimizer of L ; equivalently, if $\lim_{\tau \rightarrow 0^+} \vec{p}_\tau$ exists, then the limit belongs to minimizers of $L(\vec{p})$.

(ii) *Under Assumption B.3.* The minimizers themselves converge: $\|\vec{p}_\tau - \vec{p}_o\|_2 \rightarrow 0$ as $\tau \rightarrow 0^+$. Moreover, combining Corollary B.8 with Theorem B.9 yields the quantitative bound

$$\|\vec{p}_\tau - \vec{p}_o\|_2 = \mathcal{O}(\delta_\tau^{1/2}) \quad (\tau \rightarrow 0^+),$$

where $\delta_\tau := \sup_{\vec{p} \in P_o} |L_\tau^{1/2}(\vec{p}) - L^{1/2}(\vec{p})|$.

paragraphRemark DePCoN does not explicitly compute $\arg \min L_\tau$ for each τ . Rather, it minimizes an aggregated multi-scale loss that couples parameter estimates across smoothing levels through a learned predictor. The consistency result above suggests that, when the multi-scale loss is well-optimized, the learned parameters are encouraged to remain close to the family of minimizers of L_τ , thereby stabilizing convergence toward the $\tau \rightarrow 0$ regime.

Lemma B.4. *Let $S \in \mathcal{L}^2(\mathbb{R})$ be an input supported on $[0, T]$, extended by 0 to $\mathbb{R} \setminus [0, T]$. Assume that $\{K_\tau\}_{\tau>0} \subset C^\infty(\mathbb{R})$ is a family of nonnegative kernels satisfying*

$$\int_{\mathbb{R}} K_\tau(t) dt = 1 \quad \forall \tau > 0, \quad \text{and} \quad \lim_{\tau \rightarrow 0^+} \int_{|t|>\delta} K_\tau(t) dt = 0 \quad \forall \delta > 0. \quad (10)$$

Then $\|K_\tau * S - S\|_{\mathcal{L}^2(\mathbb{R})} \rightarrow 0$ as $\tau \rightarrow 0^+$, where, for each $\tau > 0$,

$$(K_\tau * S)(t) = \int_{-\infty}^{\infty} K_\tau(t-s) S(s) ds,$$

and $K_\tau * S \in C^\infty(\mathbb{R})$.

Proof. This is a standard approximation-to-the-identity result in $\mathcal{L}^2(\mathbb{R})$; see, (Stein & Shakarchi, 2009; Brezis & Brézis, 2011). \square

Corollary B.5. *Let*

$$K_\tau(t) = \frac{1}{\sqrt{4\pi\tau}} \exp\left(-\frac{t^2}{4\tau}\right)$$

be the heat kernel and define $S_\tau := K_\tau * S$. Suppose $S \in \mathcal{L}^2(\mathbb{R})$ and S is supported on $[0, T]$. Then:

$$i) \|S_\tau - S\|_{\mathcal{L}^2(\mathbb{R})} \rightarrow 0 \text{ as } \tau \rightarrow 0^+, \quad (11)$$

$$ii) \|S_\tau\|_{\mathcal{L}^2(\mathbb{R})} \rightarrow 0 \text{ as } \tau \rightarrow \infty. \quad (12)$$

Proof. i) The heat kernel K_τ satisfies Equation (10). Therefore, by Lemma B.4,

$$\|S_\tau - S\|_{\mathcal{L}^2(\mathbb{R})} \rightarrow 0 \text{ as } \tau \rightarrow 0^+.$$

ii) Since S is supported on $[0, T]$, we have $S \in \mathcal{L}^1(\mathbb{R})$ (\mathcal{L}^p embedding). By Young's inequality,

$$\|S_\tau\|_{\mathcal{L}^2(\mathbb{R})} = \|K_\tau * S\|_{\mathcal{L}^2(\mathbb{R})} \leq \|K_\tau\|_{\mathcal{L}^2(\mathbb{R})} \|S\|_{\mathcal{L}^1(\mathbb{R})}.$$

For the heat kernel, $\|K_\tau\|_{\mathcal{L}^2(\mathbb{R})} \propto \tau^{-1/4}$, and hence $\|S_\tau\|_{\mathcal{L}^2(\mathbb{R})} \rightarrow 0$ as $\tau \rightarrow \infty$. \square

Lemma B.6. Fix $\vec{p} \in P_o$ and $\tau_1, \tau_2 > 0$. Let $\vec{y}_{\tau_1}(t) = \vec{y}_{\tau_1}(t; \vec{p})$ and $\vec{y}_{\tau_2}(t) = \vec{y}_{\tau_2}(t; \vec{p})$ denote the solutions of Equation (4) driven by the smoothed inputs S_{τ_1} and S_{τ_2} , respectively, with the same initial condition as the observation. That is,

$$\frac{d}{dt} \vec{y}_{\tau_1}(t) = F(\vec{y}_{\tau_1}(t), \vec{p}, S_{\tau_1}(t)), \quad (13)$$

$$\frac{d}{dt} \vec{y}_{\tau_2}(t) = F(\vec{y}_{\tau_2}(t), \vec{p}, S_{\tau_2}(t)), \quad (14)$$

$$\vec{y}_{\tau_1}(0) = \vec{y}_{\tau_2}(0) = \vec{y}_o(0). \quad (15)$$

Then, under Assumption B.2, the following stability estimate holds:

$$\|\vec{y}_{\tau_1}(\cdot; \vec{p}) - \vec{y}_{\tau_2}(\cdot; \vec{p})\|_{\mathcal{L}^2([0, T])} \leq C(T) \|S_{\tau_1} - S_{\tau_2}\|_{\mathcal{L}^2([0, T])}, \quad (16)$$

where the constant $C(T) > 0$ depends only on C_1, C_2 , and the terminal time $T \in (0, \infty)$.

Proof. Subtracting Equation (14) from Equation (13) and integrating over $[0, t]$ yield

$$\begin{aligned} \vec{y}_{\tau_1}(t) - \vec{y}_{\tau_2}(t) &= \int_0^t \left(F(\vec{y}_{\tau_1}(v), \vec{p}, S_{\tau_1}(v)) - F(\vec{y}_{\tau_1}(v), \vec{p}, S_{\tau_2}(v)) \right) dv \\ &\quad + \int_0^t \left(F(\vec{y}_{\tau_1}(v), \vec{p}, S_{\tau_2}(v)) - F(\vec{y}_{\tau_2}(v), \vec{p}, S_{\tau_2}(v)) \right) dv, \end{aligned}$$

where we used the initial condition Equation (15) to simplify the left-hand side.

Taking L^2 norms, squaring both sides, and applying $(a + b)^2 \leq 2(a^2 + b^2)$, we obtain

$$\begin{aligned} \frac{1}{2} \|\vec{y}_{\tau_1}(t) - \vec{y}_{\tau_2}(t)\|_2^2 &\leq \left\| \int_0^t \left[F(\vec{y}_{\tau_1}(v), \vec{p}, S_{\tau_1}(v)) - F(\vec{y}_{\tau_1}(v), \vec{p}, S_{\tau_2}(v)) \right] dv \right\|_2^2 \\ &\quad + \left\| \int_0^t \left[F(\vec{y}_{\tau_1}(v), \vec{p}, S_{\tau_2}(v)) - F(\vec{y}_{\tau_2}(v), \vec{p}, S_{\tau_2}(v)) \right] dv \right\|_2^2. \end{aligned} \quad (17)$$

By Hölder's inequality and Assumption B.2, the first term on the right-hand side of Equation (17) is bounded as

$$\begin{aligned} \left\| \int_0^t \left[F(\vec{y}_{\tau_1}(v), \vec{p}, S_{\tau_1}(v)) - F(\vec{y}_{\tau_1}(v), \vec{p}, S_{\tau_2}(v)) \right] dv \right\|_2^2 &\leq C_2^2 t \int_0^t |S_{\tau_1}(v) - S_{\tau_2}(v)|^2 dv \\ &\leq C_2^2 T \int_0^t |S_{\tau_1}(v) - S_{\tau_2}(v)|^2 dv. \end{aligned} \quad (18)$$

where C_2 is the global constant as in the Assumption B.2. Similarly, the second term on the right-hand side of Equation (17) admits the bound

$$\left\| \int_0^t \left[F(\vec{y}_{\tau_1}(v), \vec{p}, S_{\tau_2}(v)) - F(\vec{y}_{\tau_2}(v), \vec{p}, S_{\tau_2}(v)) \right] dv \right\|_2^2 \leq C_1^2 T \int_0^t \|\vec{y}_{\tau_1}(v) - \vec{y}_{\tau_2}(v)\|_2^2 dv. \quad (19)$$

By combining Equation (17), Equation (18), and Equation (19), we obtain

$$\|\vec{y}_{\tau_1}(t) - \vec{y}_{\tau_2}(t)\|_2^2 \leq \tilde{C}(T) \left(\int_0^t |S_{\tau_1}(v) - S_{\tau_2}(v)|^2 dv + \int_0^t \|\vec{y}_{\tau_1}(v) - \vec{y}_{\tau_2}(v)\|_2^2 dv \right), \quad (20)$$

where one may take $\tilde{C}(T) = 2T \max\{C_2^2, C_1^2\}$.

Applying Grönwall's inequality (Ye et al., 2007) to Equation (20) on $[0, T]$ yields, for all $t \in [0, T]$,

$$\|\vec{y}_{\tau_1}(t) - \vec{y}_{\tau_2}(t)\|_2^2 \leq \tilde{C}(T) \int_0^t |S_{\tau_1}(v) - S_{\tau_2}(v)|^2 dv.$$

Integrating this estimate over $t \in [0, T]$ gives

$$\|\vec{y}_{\tau_1}(\cdot; \vec{p}) - \vec{y}_{\tau_2}(\cdot; \vec{p})\|_{\mathcal{L}^2([0, T])} \leq C(T) \|S_{\tau_1} - S_{\tau_2}\|_{\mathcal{L}^2([0, T])},$$

which proves Equation (16). \square

Corollary B.7. Let $L_\tau(\vec{p})$ and $L(\vec{p})$ be the losses defined in Equation (8) and Equation (9), respectively. Then

$$\|L_\tau^{1/2} - L^{1/2}\|_{\mathcal{L}^2(P_o)} \leq C \|S_\tau - S\|_{\mathcal{L}^2([0, T])}, \quad (21)$$

where the constant $C > 0$ depends only on the terminal time T and the set P_o .

Proof. We first bound $|L_\tau^{1/2}(\vec{p}) - L^{1/2}(\vec{p})|$. By the reverse triangle inequality in $\mathcal{L}^2([0, T])$,

$$\begin{aligned} |L_\tau^{1/2}(\vec{p}) - L^{1/2}(\vec{p})| &= \left| \|\vec{y}_\tau(\cdot; \vec{p}) - \vec{y}_o(\cdot)\|_{\mathcal{L}^2([0, T])} - \|\vec{y}(\cdot; \vec{p}) - \vec{y}_o(\cdot)\|_{\mathcal{L}^2([0, T])} \right| \\ &\leq \|\vec{y}_\tau(\cdot; \vec{p}) - \vec{y}(\cdot; \vec{p})\|_{\mathcal{L}^2([0, T])} \leq C(T) \|S_\tau - S\|_{\mathcal{L}^2([0, T])}, \end{aligned} \quad (22)$$

where the last inequality follows from Lemma B.6 (with $\tau_1 = \tau$ and $\tau_2 = 0$, i.e., $S_{\tau_2} = S$).

Squaring both sides of Equation (22) and integrating over $\vec{p} \in P_o$ yield

$$\|L_\tau^{1/2} - L^{1/2}\|_{\mathcal{L}^2(P_o)} \leq C(T) |P_o|^{1/2} \|S_\tau - S\|_{\mathcal{L}^2([0, T])},$$

where $|P_o|$ denotes the Lebesgue measure of P_o . By Assumption B.1, P_o is compact in \mathbb{R}^{d_p} and hence has finite measure. \square

Corollary B.8. Given $S \in \mathcal{L}^2(\mathbb{R})$, let $\delta_\tau := \sup_{\vec{p} \in P_o} |L_\tau^{1/2}(\vec{p}) - L^{1/2}(\vec{p})|$. Then, for any $T \in (0, \infty)$, δ_τ is uniformly bounded over $\tau > 0$. That is, there exists a constant $M > 0$ such that

$$0 \leq \delta_\tau \leq M, \quad \forall \tau > 0.$$

Proof. Recall Equation (22):

$$|L_\tau^{1/2}(\vec{p}) - L^{1/2}(\vec{p})| \leq C(T) \|S_\tau - S\|_{\mathcal{L}^2([0, T])}.$$

By Equation (12) in Corollary B.5, $\|S_\tau\|_{\mathcal{L}^2(\mathbb{R})} \rightarrow 0$ as $\tau \rightarrow \infty$, and hence $\sup_{\tau > 0} \|S_\tau\|_{\mathcal{L}^2(\mathbb{R})} < \infty$. Let

$$M_1 := \sup_{\tau > 0} \|S_\tau\|_{\mathcal{L}^2(\mathbb{R})}.$$

Then, for all $\tau > 0$,

$$\|S_\tau - S\|_{\mathcal{L}^2([0, T])} \leq \|S_\tau\|_{\mathcal{L}^2([0, T])} + \|S\|_{\mathcal{L}^2([0, T])} \leq M_1 + \|S\|_{\mathcal{L}^2([0, T])}.$$

Therefore,

$$|L_\tau^{1/2}(\vec{p}) - L^{1/2}(\vec{p})| \leq C(T) (M_1 + \|S\|_{\mathcal{L}^2([0, T])}) =: M,$$

and taking the supremum over $\vec{p} \in P_o$ proves the claim. \square

Theorem B.9. Let $\vec{p}_\tau \in P_o$ be a minimizer of L_τ for each $\tau > 0$.

(i) Without Assumption B.3. We have

$$\lim_{\tau \rightarrow 0^+} L(\vec{p}_\tau) = L(\vec{p}_o).$$

In particular, if the limit $\lim_{\tau \rightarrow 0^+} \vec{p}_\tau$ exists, then it belongs to the set of global minimizers of L on P_o , i.e.,

$$\lim_{\tau \rightarrow 0^+} \vec{p}_\tau \in \arg \min_{\vec{p} \in P_o} L(\vec{p}).$$

(ii) Under Assumption B.3. We further have

$$\vec{p}_\tau \rightarrow \vec{p}_o \quad \text{as } \tau \rightarrow 0^+,$$

and there exists a constant $C > 0$ such that

$$\|\vec{p}_\tau - \vec{p}_o\|_2 \leq C \delta_\tau, \quad \tau \rightarrow 0^+,$$

where $\delta_\tau = \sup_{\vec{p} \in P_o} |L_\tau^{1/2}(\vec{p}) - L^{1/2}(\vec{p})|$.

Proof. Since \vec{p}_τ minimizes $L_\tau^{1/2}$ on P_o ,

$$L_\tau^{1/2}(\vec{p}_\tau) \leq L_\tau^{1/2}(\vec{p}_o).$$

By definition of δ_τ , for any $\vec{p} \in P_o$,

$$|L_\tau^{1/2}(\vec{p}) - L^{1/2}(\vec{p})| \leq \delta_\tau.$$

Hence,

$$\begin{aligned} L^{1/2}(\vec{p}_\tau) &\leq |L^{1/2}(\vec{p}_\tau) - L_\tau^{1/2}(\vec{p}_\tau)| + L_\tau^{1/2}(\vec{p}_\tau) \\ &\leq \delta_\tau + L_\tau^{1/2}(\vec{p}_o) \\ &\leq \delta_\tau + |L_\tau^{1/2}(\vec{p}_o) - L^{1/2}(\vec{p}_o)| + L^{1/2}(\vec{p}_o) \\ &\leq 2\delta_\tau + L^{1/2}(\vec{p}_o). \end{aligned}$$

Since \vec{p}_o minimizes $L^{1/2}$, we also have $L^{1/2}(\vec{p}_o) \leq L^{1/2}(\vec{p}_\tau)$. Therefore,

$$0 \leq L^{1/2}(\vec{p}_\tau) - L^{1/2}(\vec{p}_o) \leq 2\delta_\tau.$$

Because $\delta_\tau \rightarrow 0$ as $\tau \rightarrow 0^+$ (by Corollary B.7), this proves (i).

Now assume Assumption B.3. Since $L^{1/2}(\vec{p}_\tau) - L^{1/2}(\vec{p}_o) \geq c\|\vec{p}_\tau - \vec{p}_o\|_2^2$, we have

$$\|\vec{p}_\tau - \vec{p}_o\|_2 \leq c^{-1/2} (L^{1/2}(\vec{p}_\tau) - L^{1/2}(\vec{p}_o)) \leq \sqrt{\frac{2}{c}} \delta_\tau^{1/2}.$$

Thus $\vec{p}_\tau \rightarrow \vec{p}_o$ as $\tau \rightarrow 0^+$, with the rate $\delta_\tau^{1/2}$. □

C. Error Estimate

The previous section describes the limiting behavior of the ideal stationary branch $\{\vec{p}_\tau\}$ in the kernel-based smoothing framework for each smoothing level $\tau > 0$. While that analysis assumes access to the exact local minimizer \vec{p}_τ of L_τ , in practice the corrector step in DePCoN produces only numerical parameter estimates $\{\hat{p}_{\tau_n}\}_{n=1}^N$ obtained by running a finite number of iterations of a gradient-based optimizer. This iteration is terminated once a prescribed stopping criterion is satisfied, as described in Section 4.4,

$$\|\nabla_{\vec{p}} L_{\tau_n}(\hat{p}_{\tau_n})\|_2 \leq \varepsilon_n, \quad (23)$$

where $\varepsilon_n > 0$ is a user-defined tolerance. As a result, the computed estimate \hat{p}_{τ_n} may differ from the exact minimizer \vec{p}_{τ_n} , leading to a corrector error (24)

$$\vec{e}_{\tau_n} := \hat{p}_{\tau_n} - \vec{p}_{\tau_n}. \quad (24)$$

at level τ_n . In addition, even if the exact stationary point \vec{p}_{τ_n} were provided as input to the predictor, the learned network may not map it exactly to the next stationary point $\vec{p}_{\tau_{n-1}}$. We quantify this intrinsic predictor mismatch $\vec{\beta}_{\tau_n}$ (25) along the stationary branch by

$$\vec{\beta}_{\tau_n} := f_\theta(\vec{p}_{\tau_n}) - \vec{p}_{\tau_{n-1}}. \quad (25)$$

This term reflects the approximation accuracy of the predictor network with respect to the ideal one-step continuation along the stationary branch.

The predictor step in DePCoN propagates parameter estimates across smoothing levels from τ_n to τ_{n-1} (see Section 4.3). Since this propagation is performed over a finite step size $\Delta\tau_n := \tau_n - \tau_{n-1}$, it introduces an additional τ -discretization error. In the following, we analyze how these two sources of error accumulate across smoothing levels in terms of estimation accuracy.

The error analysis is organized into four steps. While the convergence results in Section B describe the limiting behavior of the ideal stationary branch $\{\vec{p}_\tau\}$, the following steps quantify how closely the numerical estimates $\{\hat{p}_{\tau_n}\}$ track this branch under finite optimization accuracy and finite τ -discretization.

Step C.1 (Differentiability of L_τ for $\tau > 0$). Under Assumption B.2 and Lemma B.4 (smoothness of S_τ), for each fixed $\tau > 0$, the trajectory map $\vec{p} \mapsto \vec{y}_\tau(\cdot; \vec{p})$ is continuously differentiable. Consequently, the loss $L_\tau(\vec{p})$ is continuously differentiable on P_o , and $\nabla_{\vec{p}} L_\tau$ is well-defined. This justifies the stopping criterion (23) and ensures that local Taylor expansions of $\nabla_{\vec{p}} L_\tau$ are valid. (Lemma C.1.)

Step C.2 (Local nondegeneracy and continuation stability). Assume that along the selected stationary branch $\{\vec{p}_\tau\}$, the Hessian $\nabla_{\vec{p}}^2 L_\tau(\vec{p}_\tau)$ is invertible for $\tau > 0$ (local non-degeneracy condition). The stationary branch is then locally differentiable with respect to τ and satisfies a continuation equation of the form

$$\frac{d}{d\tau} \vec{p}_\tau = -(\nabla_{\vec{p}}^2 L_\tau(\vec{p}_\tau))^{-1} \partial_\tau \nabla_{\vec{p}} L_\tau(\vec{p}_\tau).$$

In particular, there exists a constant $C_n > 0$ such that

$$\|\vec{p}_{\tau_n} - \vec{p}_{\tau_{n-1}}\|_2 \leq C_n |\Delta\tau_n|.$$

This bound quantifies the intrinsic movement of the exact minimizers across smoothing levels. (Lemma C.2 and Corollary C.3)

Step C.3 (Corrector error bound at each smoothing level). Let \hat{p}_{τ_n} satisfy (23). Under the local non-degeneracy condition in Step C.2, we obtain the local estimate

$$\|\vec{e}_{\tau_n}\|_2 \leq \kappa_n \varepsilon_n,$$

for sufficiently small ε_n , where $\vec{e}_{\tau_n} = \hat{p}_{\tau_n} - \vec{p}_{\tau_n}$. This step quantifies the deviation induced by finite optimization accuracy at level τ_n . (Lemma C.4)

Step C.4 (Predictor-corrector one-step error recursion). Combining the corrector bound from Step C.3 with the intrinsic predictor mismatch $\vec{\beta}_{\tau_n}$, we obtain the one-step tracking estimate

$$\|\vec{e}_{\tau_{n-1}}\|_2 \leq \kappa_{n-1} \varepsilon_{n-1} + L_n \|\vec{e}_{\tau_n}\|_2 + \|\vec{\beta}_{\tau_n}\|_2,$$

where

$$\kappa_{n-1} := \left\| \left(\nabla_{\vec{p}}^2 L_{\tau_{n-1}}(\vec{p}_{\tau_{n-1}} + \xi_{n-1} \vec{e}_{\tau_{n-1}}) \right)^{-1} \right\|_2, \quad \vec{\beta}_{\tau_n} := f_\theta(\vec{p}_{\tau_n}) - \vec{p}_{\tau_{n-1}}.$$

This recursion describes how the corrector residual ε_{n-1} , the propagated error \vec{e}_{τ_n} , and the predictor mismatch $\vec{\beta}_{\tau_n}$ jointly determine the tracking accuracy at the next smoothing level. (Theorem C.5)

Lemma C.1. *The loss $L_\tau(\vec{p}) = \int_0^T \|\vec{y}_\tau(t; \vec{p}) - \vec{y}_o(t)\|_2^2 dt$ in (8) is continuously differentiable on P_o , and $\nabla_{\vec{p}} L_\tau(\vec{p})$ is well-defined.*

Proof. Since F is C^1 in (\vec{y}, \vec{p}) (Assumption B.2), the parameter sensitivity

$$Z_\tau(t; \vec{p}) := \partial_{\vec{p}} \vec{y}_\tau(t; \vec{p}) \in \mathbb{R}^{d_y \times d_p}$$

exists and is characterized as the unique solution of the sensitivity equation

$$\begin{aligned} \frac{d}{dt} Z_\tau(t; \vec{p}) &= \partial_{\vec{y}} F(\vec{y}_\tau(t; \vec{p}), \vec{p}, S_\tau(t)) Z_\tau(t; \vec{p}) + \partial_{\vec{p}} F(\vec{y}_\tau(t; \vec{p}), \vec{p}, S_\tau(t)), \\ Z_\tau(0; \vec{p}) &= \vec{0}. \end{aligned} \quad (26)$$

Here $\partial_{\vec{y}} F(\cdot)$ and $\partial_{\vec{p}} F(\cdot)$ denote the Jacobians of F with respect to \vec{y} and \vec{p} , respectively. Under Assumption B.2 and Lemma B.4, the coefficients in (26) are continuous in t along the trajectory $\vec{y}_\tau(t; \vec{p})$, so (26) is a linear ODE with a unique solution on $[0, T]$. Hence the solution map $\vec{p} \mapsto \vec{y}_\tau(\cdot; \vec{p})$ is continuously differentiable; see, e.g., (Khalil & Grizzle, 2002).

Consequently, for each fixed $\tau > 0$, the loss $L_\tau(\vec{p}) = \int_0^T \|\vec{y}_\tau(t; \vec{p}) - \vec{y}_o(t)\|_2^2 dt$ is continuously differentiable with respect to \vec{p} on P_o . Then, by applying chain rule,

$$\nabla_{\vec{p}} L_\tau(\vec{p}) = 2 \int_0^T Z_\tau(t; \vec{p})^\top (\vec{y}_\tau(t; \vec{p}) - \vec{y}_o(t)) dt. \quad (27)$$

Since $Z_\tau(t; \vec{p})$ is the solution of (26), $\nabla_{\vec{p}} L_\tau(\vec{p})$ is well-defined for all $\vec{p} \in P_o$ and $\tau > 0$. \square

Lemma C.2. *Under Assumption B.1, let $\{\vec{p}_\tau\}_{\tau \in (0, \tau_*)}$ be a family of stationary points satisfying $\nabla_{\vec{p}} L_\tau(\vec{p}_\tau) = \vec{0}$, and assume that the Hessian $\nabla_{\vec{p}}^2 L_\tau(\vec{p}_\tau)$ exists and is invertible for all $\tau \in (0, \tau_*)$. Then the mapping $\tau \mapsto \vec{p}_\tau$ is locally continuously differentiable on $(0, \tau_*)$. Moreover, \vec{p}_τ satisfies the continuation equation*

$$\frac{d}{d\tau} \vec{p}_\tau = -(\nabla_{\vec{p}}^2 L_\tau(\vec{p}_\tau))^{-1} \partial_\tau \nabla_{\vec{p}} L_\tau(\vec{p}_\tau).$$

Proof. Define $G(\vec{p}, \tau) := \nabla_{\vec{p}} L_\tau(\vec{p})$. By Lemma C.1 L_τ is continuously differentiable in \vec{p} , and hence G is continuously differentiable in (\vec{p}, τ) for $\tau > 0$. Since $G(\vec{p}_\tau, \tau) = \vec{0}$ and $\nabla_{\vec{p}} G(\vec{p}_\tau, \tau) = \nabla_{\vec{p}}^2 L_\tau(\vec{p}_\tau)$, the implicit function theorem implies \vec{p}_τ depends differentiably on τ . That is, differentiating the identity $G(\vec{p}_\tau, \tau) = \vec{0}$ with respect to τ yields

$$\nabla_{\vec{p}}^2 L_\tau(\vec{p}_\tau) \frac{d}{d\tau} \vec{p}_\tau + \partial_\tau \nabla_{\vec{p}} L_\tau(\vec{p}_\tau) = \vec{0},$$

from which the continuation equation follows. \square

Corollary C.3. *Under the setting of Lemma C.2, the stationary branch $\tau \mapsto \vec{p}_\tau$ is locally Lipschitz on $(0, \tau_*)$. In particular, for any consecutive levels $\tau_{n-1} < \tau_n < \tau_*$, there exists $\xi_n \in (\tau_{n-1}, \tau_n)$ such that*

$$\vec{p}_{\tau_n} - \vec{p}_{\tau_{n-1}} = \frac{d}{d\tau} \vec{p}_{\xi_n} (\tau_n - \tau_{n-1}).$$

Consequently,

$$\|\vec{p}_{\tau_n} - \vec{p}_{\tau_{n-1}}\|_2 \leq C_n |\Delta\tau_n|,$$

where $\Delta\tau_n := \tau_n - \tau_{n-1}$ and $C_n := \sup_{\tau \in [\tau_{n-1}, \tau_n]} \left\| \frac{d}{d\tau} \vec{p}_\tau \right\|_2 < \infty$.

Lemma C.4. Fix $n \in \{0, \dots, N\}$ and let \vec{p}_{τ_n} be the selected stationary point on the branch in Lemma C.2 and let \hat{p}_{τ_n} be a parameter estimate from DePCoN. Define the error $\vec{e}_{\tau_n} := \hat{p}_{\tau_n} - \vec{p}_{\tau_n}$. Assume that L_{τ_n} is three times continuously differentiable in a neighborhood of \vec{p}_{τ_n} .

Then there exists $\xi_{\tau_n} \in (0, 1)$ such that

$$\nabla_{\vec{p}} L_{\tau_n}(\hat{p}_{\tau_n}) = \nabla_{\vec{p}}^2 L_{\tau_n}(\vec{p}_{\tau_n} + \xi_{\tau_n} \vec{e}_{\tau_n}) \vec{e}_{\tau_n}.$$

If the Hessian is invertible at $\vec{p}_{\tau_n} + \xi_{\tau_n} \vec{e}_{\tau_n}$, then

$$\vec{e}_{\tau_n} = \nabla_{\vec{p}}^2 L_{\tau_n}(\vec{p}_{\tau_n} + \xi_{\tau_n} \vec{e}_{\tau_n})^{-1} \nabla_{\vec{p}} L_{\tau_n}(\hat{p}_{\tau_n}),$$

and hence

$$\|\vec{e}_{\tau_n}\|_2 \leq \kappa_n \varepsilon_n,$$

where $\kappa_n := \left\| \nabla_{\vec{p}}^2 L_{\tau_n}(\vec{p}_{\tau_n} + \xi_{\tau_n} \vec{e}_{\tau_n})^{-1} \right\|_2$.

Proof. Since \vec{p}_τ is stationary, $G(\vec{p}_\tau) = \vec{0}$. Apply the (vector-valued) mean value theorem to G along the segment $\vec{p}_\tau + s\vec{e}_\tau$, $s \in [0, 1]$: there exists $\xi_\tau \in (0, 1)$ such that

$$G(\hat{p}_\tau) - G(\vec{p}_\tau) = \nabla_{\vec{p}} G(\vec{p}_\tau + \xi_\tau \vec{e}_\tau) \vec{e}_\tau.$$

Recalling that $\nabla_{\vec{p}} G(\vec{p}) = \nabla_{\vec{p}}^2 L_\tau(\vec{p})$, we obtain

$$\nabla_{\vec{p}} L_\tau(\hat{p}_\tau) = \nabla_{\vec{p}}^2 L_\tau(\vec{p}_\tau + \xi_\tau \vec{e}_\tau) \vec{e}_\tau,$$

which proves the claimed identity.

If $\nabla_{\vec{p}}^2 L_\tau(\vec{p}_\tau + \xi_\tau \vec{e}_\tau)$ is invertible, then we can solve for \vec{e}_τ :

$$\vec{e}_\tau = \left(\nabla_{\vec{p}}^2 L_\tau(\vec{p}_\tau + \xi_\tau \vec{e}_\tau) \right)^{-1} \nabla_{\vec{p}} L_\tau(\hat{p}_\tau).$$

Taking the Euclidean operator norm gives

$$\|\vec{e}_\tau\|_2 \leq \left\| \left(\nabla_{\vec{p}}^2 L_\tau(\vec{p}_\tau + \xi_\tau \vec{e}_\tau) \right)^{-1} \right\|_2 \|\nabla_{\vec{p}} L_\tau(\hat{p}_\tau)\|_2.$$

Finally, if $\|\nabla_{\vec{p}} L_\tau(\hat{p}_\tau)\|_2 \leq \varepsilon_n$, the stated bound $\|\vec{e}_{\tau_n}\|_2 \leq \kappa_n \varepsilon_n$ follows. \square

Remark. Since the predictor f_θ is a feed-forward network composed of affine maps and ReLU activations (see Section 4.3), it is piecewise affine and hence Lipschitz continuous on any compact set. In particular, on the compact admissible set P_o , there exists a constant $L \geq 0$ such that

$$\|f_\theta(\vec{p}) - f_\theta(\vec{q})\|_2 \leq L \|\vec{p} - \vec{q}\|_2, \quad \forall \vec{p}, \vec{q} \in P_o.$$

Under this property, we have the following theorem.

Theorem C.5. Fix $n \in \{1, \dots, N\}$. Assume the selected stationary branch $\{\vec{p}_{\tau_k}\}_{k=0}^N$ is well-defined, and suppose the corrector output $\hat{p}_{\tau_{n-1}}$ satisfies the stopping criterion

$$\|\nabla_{\vec{p}} L_{\tau_{n-1}}(\hat{p}_{\tau_{n-1}})\|_2 \leq \varepsilon_{n-1}.$$

Assume further that the Hessian is invertible along the line segment between $\vec{p}_{\tau_{n-1}}$ and $\hat{p}_{\tau_{n-1}}$, i.e.,

$$\nabla_{\vec{p}}^2 L_{\tau_{n-1}}(\vec{p}_{\tau_{n-1}} + s \vec{e}_{\tau_{n-1}}) \text{ is invertible for all } s \in [0, 1],$$

where $\vec{e}_{\tau_{n-1}} := \hat{p}_{\tau_{n-1}} - \vec{p}_{\tau_{n-1}}$.

Then the tracking error satisfies the one-step bound

$$\|\vec{e}_{\tau_{n-1}}\|_2 \leq \kappa_{n-1} \varepsilon_{n-1} + L_n \|\vec{e}_{\tau_n}\|_2 + \|\vec{\beta}_{\tau_n}\|_2,$$

where

$$\kappa_{n-1} := \left\| \left(\nabla_{\vec{p}}^2 L_{\tau_{n-1}}(\vec{p}_{\tau_{n-1}} + \xi_{n-1} \vec{e}_{\tau_{n-1}}) \right)^{-1} \right\|_2, \quad \vec{\beta}_n := f_\theta(\vec{p}_{\tau_n}) - \vec{p}_{\tau_{n-1}}.$$

Proof. We start from the predictor recursion

$$\hat{p}_{\tau_{n-1}} = f_\theta(\hat{p}_{\tau_n}), \quad \vec{e}_{\tau_k} := \hat{p}_{\tau_k} - \vec{p}_{\tau_k}.$$

Insert and subtract $f_\theta(\vec{p}_{\tau_n})$ to decompose the error at level τ_{n-1} :

$$\begin{aligned} \vec{e}_{\tau_{n-1}} &= \hat{p}_{\tau_{n-1}} - \vec{p}_{\tau_{n-1}} = f_\theta(\hat{p}_{\tau_n}) - \vec{p}_{\tau_{n-1}} \\ &= (f_\theta(\hat{p}_{\tau_n}) - f_\theta(\vec{p}_{\tau_n})) + (f_\theta(\vec{p}_{\tau_n}) - \vec{p}_{\tau_{n-1}}) \\ &= (f_\theta(\hat{p}_{\tau_n}) - f_\theta(\vec{p}_{\tau_n})) + \vec{\beta}_n. \end{aligned}$$

Taking norms and using the assumed Lipschitz continuity of f_θ on P_o (with Lipschitz constant L_n at this step) yields

$$\|\vec{e}_{\tau_{n-1}}\|_2 \leq L_n \|\hat{p}_{\tau_n} - \vec{p}_{\tau_n}\|_2 + \|\vec{\beta}_n\|_2 = L_n \|\vec{e}_{\tau_n}\|_2 + \|\vec{\beta}_n\|_2.$$

It remains to incorporate the contribution of the corrector stopping criterion at level τ_{n-1} .

Since $\vec{p}_{\tau_{n-1}}$ lies on the selected stationary branch, it satisfies

$$\nabla_{\vec{p}} L_{\tau_{n-1}}(\vec{p}_{\tau_{n-1}}) = \vec{0}.$$

Apply the mean value theorem to the vector-valued map $\nabla_{\vec{p}} L_{\tau_{n-1}}(\cdot)$ along the segment $\vec{p}_{\tau_{n-1}} + s \vec{e}_{\tau_{n-1}}$ for $s \in [0, 1]$: there exists $\xi_{n-1} \in (0, 1)$ such that

$$\begin{aligned} \nabla_{\vec{p}} L_{\tau_{n-1}}(\hat{p}_{\tau_{n-1}}) &= \nabla_{\vec{p}} L_{\tau_{n-1}}(\vec{p}_{\tau_{n-1}}) + \nabla_{\vec{p}}^2 L_{\tau_{n-1}}(\vec{p}_{\tau_{n-1}} + \xi_{n-1} \vec{e}_{\tau_{n-1}}) \vec{e}_{\tau_{n-1}} \\ &= \nabla_{\vec{p}}^2 L_{\tau_{n-1}}(\vec{p}_{\tau_{n-1}} + \xi_{n-1} \vec{e}_{\tau_{n-1}}) \vec{e}_{\tau_{n-1}}. \end{aligned}$$

By the assumed invertibility of the Hessian along the segment, we may solve for $\vec{e}_{\tau_{n-1}}$:

$$\vec{e}_{\tau_{n-1}} = (\nabla_{\vec{p}}^2 L_{\tau_{n-1}}(\vec{p}_{\tau_{n-1}} + \xi_{n-1} \vec{e}_{\tau_{n-1}}))^{-1} \nabla_{\vec{p}} L_{\tau_{n-1}}(\hat{p}_{\tau_{n-1}}).$$

Taking norms and using the stopping criterion $\|\nabla_{\vec{p}} L_{\tau_{n-1}}(\hat{p}_{\tau_{n-1}})\|_2 \leq \varepsilon_{n-1}$ gives

$$\|\vec{e}_{\tau_{n-1}}\|_2 \leq \kappa_{n-1} \varepsilon_{n-1}, \quad \kappa_{n-1} := \left\| (\nabla_{\vec{p}}^2 L_{\tau_{n-1}}(\vec{p}_{\tau_{n-1}} + \xi_{n-1} \vec{e}_{\tau_{n-1}}))^{-1} \right\|_2.$$

Finally, combine the two bounds:

$$\begin{aligned} \|\vec{e}_{\tau_{n-1}}\|_2 &\leq \kappa_{n-1} \varepsilon_{n-1} + \|\vec{e}_{\tau_{n-1}}\|_2 \\ &\leq \kappa_{n-1} \varepsilon_{n-1} + L_n \|\vec{e}_{\tau_n}\|_2 + \|\vec{\beta}_n\|_2, \end{aligned}$$

which is the claimed one-step estimate. □

D. Supplementary tables and figures

Table 3. Various applications of non-autonomous dynamical systems driven by discontinuous exogenous inputs. Such abrupt or event-driven exogenous inputs frequently arise in real-world settings and pose significant challenges for learning and optimization in dynamical systems.

Category	Application	Discontinuous External Input	Reference
1. Control Theory	Traffic Signal Control	Periodic switching of traffic lights (Red/Green), discrete gating of vehicle flows.	(Aboudolas et al., 2009), (Du & Zhang, 2014)
	Demand Response & Smart Thermostats	Real-time price signals, grid load shedding	(Mathieu et al., 2012), (Chassin et al., 2015)
2. Life & Ecological sciences	Pharmacokinetics	Bolus injections, insulin pump delivery, Michaelis-Menten elimination	(Huang et al., 2012), (Song et al., 2014), (Tang & Xiao, 2007) (Shen et al., 2016), (Liu & Sun, 2022), (Gao et al., 2006)
	Bioprocess Engineering	Impulsive feeding, fed-batch fermentation control	(Bainov & Dishliev, 1990), (Meng et al., 2010), (Nie et al., 2009a), (Nie et al., 2009b)
	Ecological Systems	Impulsive ecological interventions (harvesting, pest control, nutrient pulses)	(Nelson et al., 2004) (Forger et al., 1999), (Lim et al., 2025)
	NF- κ B Signaling Pathways Circadian Clock	External stimuli (e.g. TNF- α) Light/Dark pulses, and discrete data sampling intervals from wearable devices	
3. Physics & Engineering	Aerospace	Instantaneous thrust, impulsive maneuvers	(Carter, 1991), (Carter, 2000)
	Mechanics	Vibro-impact (collisions), clock escapement energy, dry friction	(Brogliato, 1996), (Ibrahim, 2009), (Moline et al., 2012)
	Bipedal walking robot	Impact forces at foot-ground contact	(Westervelt et al., 2003)
	Waveguides	Structural discontinuities (conical/elliptical) in THz waveguides	(Heydari et al., 2019)
	DC-DC Converters Power Electronics	High-frequency On/Off switching of transistors Switching events, component faults	(Papafotiou et al., 2004), (Siddhartha et al., 2018) (Domínguez-García & Trenn, 2010)
4. Economics & Finance	Market Dynamics	Demand-supply shocks	(Stamova & Emmenegger, 2004), (Stamov et al., 2011)
	Financial Control	Central bank interventions, interest rate adjustments, transaction costs	(Cadenillas & Zapatero, 2000), (Bielecki & Pliska, 2000), (Clarida et al., 2000)
5. Neural Networks	Neural Dynamics	Spiking synaptic activity	(Stamov & Stamova, 2007)
6. Epidemiology	Non-pharmaceutical Interventions (NPIs)	Discrete policy shocks	(Flaxman et al., 2020)

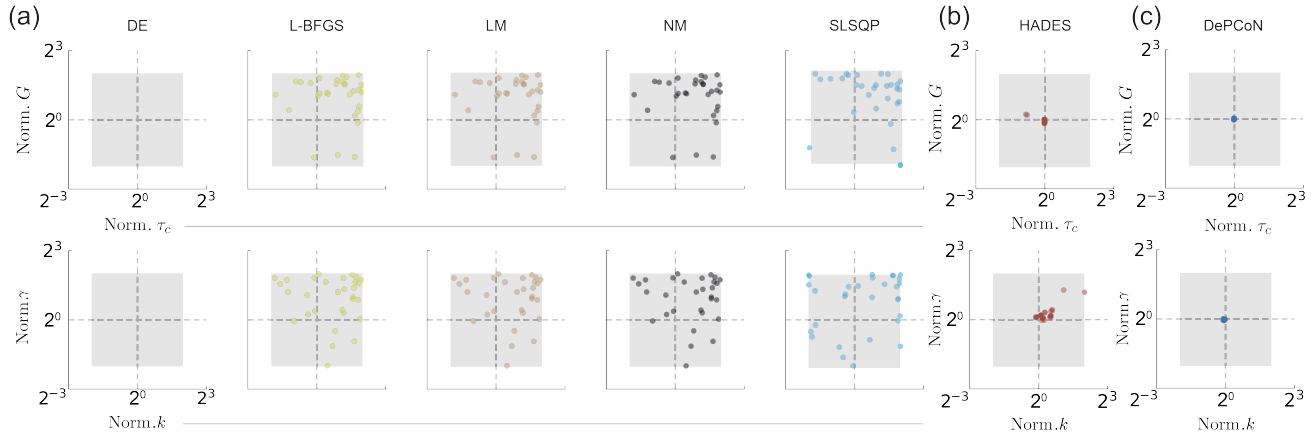


Figure 5. Comparison of parameter estimation methods on the human circadian pacemaker model introduced in Figure 1. The scatter plots summarize parameter estimates from 30 independent trials for each of seven methods (*DE*, *L-BFGS*, *LM*, *NM*, *SLSQP*, *HADES-NN*, and *DePCoN*). All parameter estimates are normalized by the true parameter values, which are located at the intersection of the dashed lines, and gray boxes indicate the parameter ranges used for random initialization. *DE* failed to produce valid parameter estimates due to numerical divergence during the search process. (a) Under discontinuous exogenous inputs, the resulting non-smooth loss landscape causes *L-BFGS*, *LM*, and *NM* to remain trapped near their initializations. (b) *HADES-NN* achieves improved estimation performance relative to these baselines, whereas (c) *DePCoN* consistently and accurately recovers the ground-truth parameter values across trials.

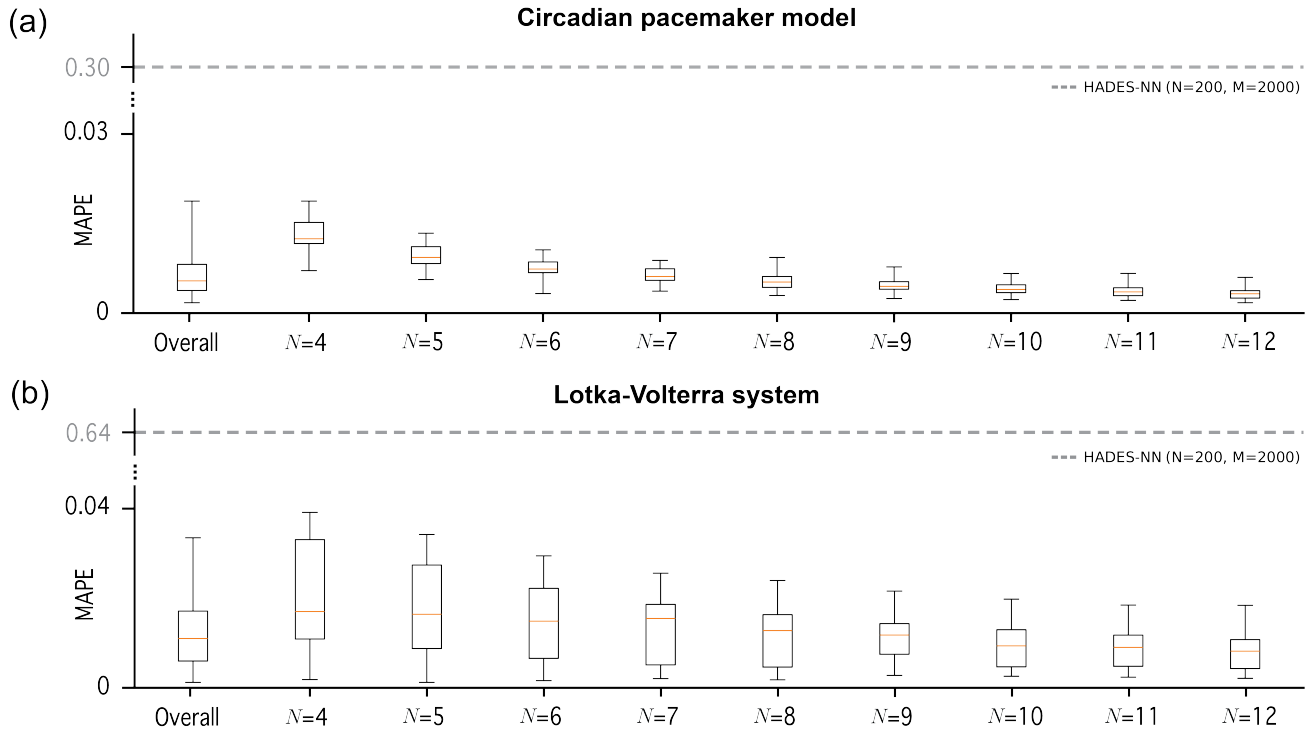


Figure 6. Sensitivity of *DePCoN* to the smoothing-grid size N . We evaluate the robustness of *DePCoN* with respect to the number of smoothing scales N using box plots of the mean absolute percentage error (MAPE). (a) Circadian pacemaker model Figure 1-(a). (b) Lotka–Volterra system Figure 4-(a). For each $N \in \{4, \dots, 12\}$, we perform 30 independent trials with random initial parameters sampled from $[p_{o,i}/4, 4p_{o,i}]$ for $i = 1, \dots, 4$. In each trial, the MAPE of the estimated parameters is computed, and its distribution is summarized as a box plot for each N . The leftmost “Overall” box plot aggregates MAPE values across all smoothing-grid sizes as a reference. The horizontal dashed line indicates the MAPE level achieved by *HADES-NN* under its reported hyperparameter setting, providing a baseline for comparison. Across both systems, *DePCoN* maintains stable MAPE distributions over a wide range of N , consistently matching or improving upon the *HADES-NN* baseline, which demonstrates strong robustness to variations in the smoothing-grid hyperparameter.